JOURNAL OF GUIDANCE, CONTROL, AND DYNAMICS
Vol. 31, No. 5, September–October 2008

Nonlinear Control of Motion Synchronization for Satellite Proximity Operations

Kamesh Subbarao*
University of Texas at Arlington, Arlington, Texas 76019-0018
and
Sam Welsh†
United Space Alliance, Houston, Texas 77058

DOI: 10.2514/1.34248

This paper considers the problem of motion synchronization of free-flying robotic spacecraft and serviceable floating objects in space. The synchronization maneuvers are a combination of relative position tracking and attitude reorientation. Control laws are developed that ensure that the relative position vector between a pursuer and target spacecraft is always directed toward the docking port of the target. The tracking-error reference signals are generated based on a novel "virtual target" construction. Also, the attitude reorientation of the pursuer is achieved by constructing a desired attitude from the virtual target, and the control law seeks to nullify the errors between the current and desired attitude parameters. The control law synthesis proceeds along familiar, established procedures motivated by feedback-linearization-based approaches. Disturbance torques due to gravity gradient and other unknown but bounded disturbances are accounted for using an adaptive control formulation. The stability of the control laws are demonstrated via Lyapunov analysis and Matrosov's theorem. Numerical simulations are performed to demonstrate the efficacy of this control formulation.

I. Introduction

THE successful capture of a tumbling object in orbit using an autonomous space vehicle has become an important research topic due to the continuous increase of orbit activity. Typical applications that could use this include collecting and removing space debris, servicing a malfunctioning satellite, refueling a powerless satellite, or installing improved technology. Researchers from the National Space Development Agency of Japan have developed a mission plan using a new system concept called the Hyper-Orbital-Servicing Vehicle (HOSV) to carry out such a phased capture. The system is composed of a bulky mothership and a deployable operation function that is agile and compact. In general, the mission of the HOSV system up to and including the point of capture is composed of five main phases: orbit transfer, approach and observation, trajectory planning, operation function deployment, and capture [1]. The scope of this paper presents techniques for observation and the control necessary to provide a safe and effective capture of a slowly tumbling satellite, which will be referred to as the target satellite. The maneuverable operation function will be referred to as the pursuer satellite and will be equipped with an onboard control system and a docking mechanism.

To gather position and state information for closed-loop control to navigate the capture vehicle toward the target, Lichter and Dubowsky [2] developed an approach that uses 3-D vision sensors during an observation phase that provides input to a Kalman filter, which extracts the full dynamic state and inertial parameters of the target. Alternately, in most missions, it is likely that the position and velocity (angular/translational) sensors in the target vehicle (assumed friendly) are operational, thereby providing the attitude and angular velocity measurements to the pursuer. In such a situation, one can precisely control the pursuer in the capture phase using an adaptive controller that compensates for the lack of the knowledge of the inertia of the target. Although in certain specific cases the identification of the target spacecraft inertia parameters might be possible, it is generally a challenging problem if the system parameters are poorly observable from the measured states and this observability cannot be guaranteed a priori.

In this paper, for the capture phase of the mission, we propose an attitude-synchronization approach combined with relative position tracking that provides an effective approach for the development of a control system to ensure a successful capture. The concept is to safely maneuver the pursuer so that its docking component is always facing the docking component of the target. While maintaining this attitude orientation through synchronization, the relative position of the satellites gradually decreases until grasping or another kind of docking is established.

Several research projects dealing with autonomous rendezvous and docking of orbiting satellites have been conducted over the past decade [3]. Particularly relevant to the work in this paper are the Tsuda and Shinichi [4] optimized control algorithm that avoids nonlinearity effects, but limits the maximum control torque for attitude synchronization of a tumbling object in space and the Nakamura et al. [5] implementation of attitude synchronization using feedback and feedforward control techniques within the same empty space environment. It seems natural that extending these approaches to the capture of a tumbling object in *any orbit* provides the most applicable scenario for today's booming satellite industry. In 1998, Mitsubishi Electric successfully docked two unmanned satellites (formally called Engineering Test Satellites VII) under the funding and direction of Japan's National Space Development Agency (JAXA). Their investigation established assurance that autonomous docking of satellites is indeed feasible and provided evidential insight for overcoming the various mishaps that can occur [6].

The rest of the paper is organized as follows: The problem description is presented in the next section, wherein the relevant coordinate frames, governing equations of motion, standing assumptions, and actuation models are detailed. Following this, the

Presented as Paper 2004-5298 at the AIAA/AAS Astrodynamics Specialist Conference and Exhibit, Providence, RI, 16–19 August 2004; received 24 August 2007; revision received 19 November 2007; accepted for publication 21 November 2007.

*Assistant Professor, Department of Mechanical and Aerospace Engineering, 500 West First Street, Box 19018, 211 Woolf Hall; subbarao@uta.edu. Life Member AIAA.

†Engineer, Navigation Department, USH-485L; Samuel.J.Welsh@usa-spaceops.com.

engagement scenario and the control methodology is described. This is followed by a discussion on the stability of the control law. Finally, detailed simulations highlighting the effectiveness of the control methodology are described.

II. Problem Description

We seek to derive globally ultimately bounded stable (in the presence of bounded disturbances) coupled position and attitude control laws for simultaneous relative position and attitude control of two spacecraft in a specified orbit. Of the two satellites in engagement, termed the *pursuer* $\mathcal{P}$ and the *target* $\mathcal{T}$, only the pursuer is maneuverable. The target is uncontrolled (rotation as well as translation) but is capable of providing its state information (position, velocity, attitude, and angular velocity) to the pursuer at all times. The following definitions and assumptions are in order.

A. Coordinate Reference Frames and Notation

For the motion of rigid spacecraft orbiting around the Earth, the following coordinate frames are considered, as shown in Fig. 1.

1) The Earth-centered coordinate frame is denoted as $\mathcal{N} = \{O_{\mathcal{N}}, \hat{i}_{\mathcal{N}}, \hat{j}_{\mathcal{N}}\hat{k}_{\mathcal{N}}\}$ and is fixed to the center of the Earth with $\hat{i}_{\mathcal{N}}$ in the direction of the vernal equinox, $\hat{k}_{\mathcal{N}}$ points toward the north pole, and $\hat{j}_{\mathcal{N}}$ (in the equatorial plane) completes the triad.

2) The local-vertical-local-horizontal (LVLH) frame attached to the target is denoted as $\mathcal{O} = \{O_{\mathcal{O}}, \hat{i}_{\mathcal{O}}, \hat{j}_{\mathcal{O}}, \hat{k}_{\mathcal{O}}\}$, where $\hat{k}_{\mathcal{O}}$ is the direction of the orbit normal, $\hat{i}_{\mathcal{O}}$ is directed along the radius vector of the target from the Earth's center $\boldsymbol{R}_{\mathcal{T}}$, and $\hat{j}_{\mathcal{O}} = \hat{k}_{\mathcal{O}} \times \hat{i}_{\mathcal{O}}$ completes the triad.

3) The body-fixed frames are denoted as $\mathcal{P} = \{O_{\mathcal{P}}, \hat{i}_{\mathcal{P}}, \hat{j}_{\mathcal{P}}\hat{k}_{\mathcal{P}}\}$ and $\mathcal{T} = \{O_{\mathcal{T}}, \hat{i}_{\mathcal{T}}, \hat{j}_{\mathcal{T}}\hat{k}_{\mathcal{T}}\}$ for the pursuer and the target, respectively. Without any loss of generality, one can assume that the fully extended docking arm denoted as $\hat{\boldsymbol{d}}_{\mathcal{P}}$ is one of the unit vectors in the triad representing the pursuer body-fixed frame; likewise, the outward normal at the receiving port on the target, $\hat{\boldsymbol{d}}_{\mathcal{T}}$, can be one of the unit vectors comprising the triad representing the target body-fixed coordinate system (see Fig. 2).

1) The coordinates of a vector $\boldsymbol{v}$ relative to the frame $\{*\}$ are denoted as $\boldsymbol{v}^{\{*\}}$

2) $[\boldsymbol{C}_{\mathcal{AB}}]$ denotes the direction cosine matrix between the coordinate frames $\mathcal{A}$ and $\mathcal{B}$. Thus, a transformation of a vector from frame $\mathcal{B}$ to frame $\mathcal{A}$ is accomplished as $\boldsymbol{v}^{\mathcal{A}} = [\boldsymbol{C}_{\mathcal{AB}}]\boldsymbol{v}^{\mathcal{B}}$.

3) The angular velocity vector of a frame $\mathcal{A}$ relative to $\mathcal{N}$ is denoted as $\boldsymbol{\omega}_{\mathcal{NA}}$, and its components with respect to either one of the reference frames are denoted by $\boldsymbol{\omega}^{\mathcal{N}}_{\mathcal{NA}}$ or $\boldsymbol{\omega}^{\mathcal{A}}_{\mathcal{NA}}$.

4) The specific identification of the angular velocity of the pursuer or the target relative to frame $\mathcal{N}$ is made by the notations $\boldsymbol{\omega}_{\mathcal{NP}}$ and $\boldsymbol{\omega}_{\mathcal{NT}}$, respectively.

B. Governing Equations of Motion

The relative translational motion dynamics are developed based on the relative position and velocity of the pursuer with respect to the LVLH frame fixed to the target; that is,

$$\boldsymbol{r}^{\mathcal{O}} = x\hat{i}_{\mathcal{O}} + y\hat{j}_{O} + z\hat{k}_{\mathcal{O}}$$

For a circular target orbit, these equations reduce to the Hill–Clohessy–Wiltshire equations [7,8]. The details of the governing equations for relative translation and attitude dynamics are given next.

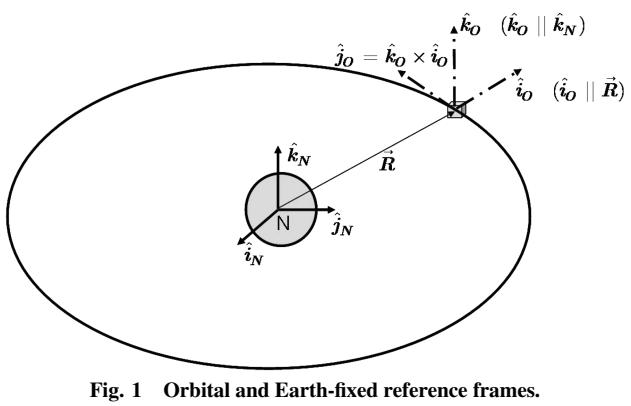

Fig. 1 Orbital and Earth-fixed reference frames.

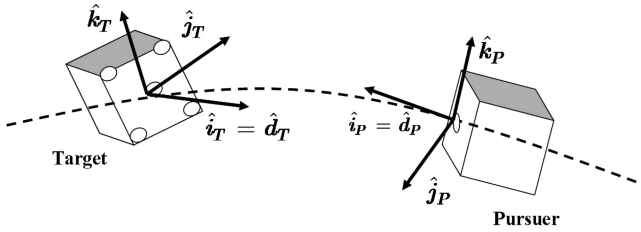

Fig. 2 Pursuer–target fixed reference frames.

1. Relative Translational Dynamics

The nonlinear equations of motion governing the translational motion are described next:

$$\ddot{x} - 2\dot{\theta}\,\dot{y} - \ddot{\theta}y - \dot{\theta}^2 x = -\frac{\mu(R_{\mathcal{T}} + x)}{((R_{\mathcal{T}} + x)^2 + y^2 + z^2)^{\frac{3}{2}}} + \frac{\mu}{R_{\mathcal{T}}^2} + u_x + f_x \tag{1}$$

$$\ddot{y} + 2\dot{\theta}\,\dot{x} + \ddot{\theta}x - \dot{\theta}^2 y = -\frac{\mu y}{((R_{\mathcal{T}} + x)^2 + y^2 + z^2)^{\frac{3}{2}}} + u_y + f_y \tag{2}$$

$$\ddot{z} = -\frac{\mu z}{((R_{\mathcal{T}} + x)^2 + y^2 + z^2)^{\frac{3}{2}}} + u_z + f_z \tag{3}$$

where $\{f_x, f_y, f_z\}$ are the relative disturbance acceleration components in the LVLH frame attached to the target and $\{u_x, u_y, u_z\}$ are the control accelerations of the pursuer with components in the target's LVLH frame. The preceding equations are augmented with those given in Eqs. (4) and (5) that describe the evolution of the target's orbit:

$$\ddot{R}_{\mathcal{T}} = R_{\mathcal{T}}\dot{\theta}^2 - \frac{\mu}{R_{\mathcal{T}}^2} \tag{4}$$

$$\ddot{\theta} = -2\frac{\dot{R}_{\mathcal{T}}}{R_{\mathcal{T}}}\dot{\theta} \tag{5}$$

where $R_{\mathcal{T}}$ is the magnitude of the radius vector to the target in the Earth-centered inertial frame $\boldsymbol{R}_{\mathcal{T}}$, and θ is the latitude angle (sum of the argument of the perigee and the true anomaly of the target satellite).

2. Rotational Dynamics

The rotational kinematics are described using a minimal parameter representation for attitude: namely, the modified Rodrigues parameters (MRPs). A detailed account of MRPs and their properties can be found in [9].

a. Target Attitude Kinematics and Dynamics. Because the attitude is parameterized in terms the modified Rodrigues parameters $\boldsymbol{\sigma}_{\mathcal{T}}$, the attitude kinematics are represented as

$$\dot{\boldsymbol{\sigma}}_{\mathcal{T}} = \tfrac{1}{4}[\boldsymbol{J}(\boldsymbol{\sigma}_{\mathcal{T}})]\boldsymbol{\omega}^{\mathcal{T}}_{\mathcal{NT}} \tag{6}$$

where $[\boldsymbol{J}(\boldsymbol{\sigma}_{\mathcal{T}})]$ is expressed as

$$[\boldsymbol{J}(\boldsymbol{\sigma}_{\mathcal{T}})] = \left[\left(1 - \boldsymbol{\sigma}_{\mathcal{T}}^T\boldsymbol{\sigma}_{\mathcal{T}}\right)I_{3\times 3} + 2\,\mathrm{skew}(\boldsymbol{\sigma}_{\mathcal{T}}) + 2\boldsymbol{\sigma}_{\mathcal{T}}\boldsymbol{\sigma}_{\mathcal{T}}^T\right]$$

The attitude dynamics are given by

$$\dot{\boldsymbol{\omega}}^{\mathcal{T}}_{\mathcal{N}\mathcal{T}} = -\boldsymbol{H}_{\mathcal{T}}^{-1}\text{skew} \tag{7}$$

where $\boldsymbol{\omega}^{\mathcal{T}}_{\mathcal{N}\mathcal{T}}$ represents the angular velocity of the target with respect to the inertial frame $\mathcal{N}$ expressed in the $\mathcal{T}$-frame components, $\boldsymbol{H}_{\mathcal{T}}$ is the moment of inertia of the target spacecraft, $\boldsymbol{\delta}_{\mathcal{T}}$ is the external disturbance torque acting on the target, and skew$(\boldsymbol{\omega}^{\mathcal{T}}_{\mathcal{N}\mathcal{T}})$ is the skew-symmetric matrix cross-product operator [7].

b. Pursuer Attitude Kinematics and Dynamics. Similar to the target, the governing equations for the pursuer's attitude dynamics are summarized next:

$$\dot{\boldsymbol{\sigma}}_{\mathcal{P}} = \tfrac{1}{4}[\boldsymbol{J}(\boldsymbol{\sigma}_{\mathcal{P}})]\boldsymbol{\omega}^{\mathcal{P}}_{\mathcal{N}\mathcal{P}} \tag{8}$$

$$\dot{\boldsymbol{\omega}}^{\mathcal{P}}_{\mathcal{N}\mathcal{P}} = -\boldsymbol{H}_{\mathcal{P}}^{-1}\,\text{skew} \tag{9}$$

where $\boldsymbol{\sigma}_{\mathcal{P}}$ is the MRP that parameterize the attitude of the pursuer, $\boldsymbol{\omega}^{\mathcal{P}}_{\mathcal{N}\mathcal{P}}$ represents the angular velocity of the pursuer with respect to the inertial frame $\mathcal{N}$ expressed in the $\mathcal{P}$-frame components, $\boldsymbol{H}_{\mathcal{P}}$ is the moment of inertia of the pursuer spacecraft, $\boldsymbol{\delta}_{\mathcal{P}}$ is the external disturbance torque acting on the pursuer, and $\boldsymbol{\tau}$ is the control torque input.

c. Disturbance Torques. The disturbance torques that are modeled include gravity gradient torques and unknown disturbances with known waveforms. We lump all these disturbances and represent them as

$$\boldsymbol{\delta}_i = \boldsymbol{\delta}_{i0} + \boldsymbol{\delta}_{ic}\cos(\lambda t) + \boldsymbol{\delta}_{is}\sin(\lambda t)$$

It is further assumed that although the orbit frequency

$$\lambda = \sqrt{\frac{\mu}{a_{\mathcal{T}}^3}}$$

(where $a_{\mathcal{T}}$ is the semimajor axis of the target's orbit) is known a priori, the disturbance amplitudes $\{\boldsymbol{\delta}_{i0}, \boldsymbol{\delta}_{ic}, \boldsymbol{\delta}_{is}\}$ are unknown ($i = \mathcal{P}$ or $\mathcal{T}$, depending on whether it is the pursuer or the target in consideration). The actuators used for the attitude control of the pursuer are assumed to be passive, such as momentum wheels:

$$\begin{aligned}\boldsymbol{\delta}_{\mathcal{P}} &= \boldsymbol{\delta}_{\mathcal{P}0} + \boldsymbol{\delta}_{\mathcal{P}c}\cos(\lambda t) + \boldsymbol{\delta}_{\mathcal{P}s}\sin(\lambda t) + \frac{\mu}{R_{\mathcal{P}}^5}\boldsymbol{R}^{\mathcal{P}}_{\mathcal{P}} \times \boldsymbol{H}_{\mathcal{P}}\boldsymbol{R}^{\mathcal{P}}_{\mathcal{P}}\\ \boldsymbol{\delta}_{\mathcal{T}} &= \boldsymbol{\delta}_{\mathcal{T}0} + \boldsymbol{\delta}_{\mathcal{T}c}\cos(\lambda t) + \boldsymbol{\delta}_{\mathcal{T}s}\sin(\lambda t) + \frac{\mu}{R_{\mathcal{T}}^5}\boldsymbol{R}^{\mathcal{T}}_{\mathcal{T}} \times \boldsymbol{H}_{\mathcal{T}}\boldsymbol{R}^{\mathcal{T}}_{\mathcal{T}}\end{aligned} \tag{10}$$

Note that because the translational motion of the target is assumed to be perturbed by disturbance forces, the orbit of the target is perturbed, and hence the orbit frequency could change, making it time-varying. We neglect these variations in the analysis. This is a reasonable assumption because the engagement times are much shorter than the period of the orbit itself.

III. Engagement Scenario and Control Methodology

The solution to the problem stated in Sec. II is achieved via precise attitude synchronization and relative position tracking. In other words, the control system onboard the pursuer adjusts the pursuer's attitude and maneuvers its relative position such that its docking port is aligned with the docking port of the target.

Note that in subsequent sections, each aspect of the control (rotation and translation) is derived separately. This is only for the sake of illustration. The actual synthesis is, in fact, a coupled control law derivation. The control strategy for this coupled position tracking and attitude synchronization is described next:

A. Relative Position Tracking

The objective for the translational control (force input) is to maintain a safe constant relative distance between the target and the pursuer. To implement this, a fictitious desired relative position vector $\boldsymbol{r}^{\mathcal{T}}_d$ is constructed. For the desired constant relative distance defined as r_d, the desired relative position vector is simply

$$\boldsymbol{r}^{\mathcal{T}}_d = r_d\hat{\boldsymbol{d}}_{\mathcal{T}} = r_d\hat{i}_{\mathcal{T}}$$

(without loss of generality). Thus, if the translational position error is defined as

$$\boldsymbol{e}^{\mathcal{O}} = \boldsymbol{r}^{\mathcal{O}} - [\boldsymbol{C}_{\mathcal{O}\mathcal{T}}]\boldsymbol{r}^{\mathcal{T}}_d$$

then the objective of the control law is to ensure that $\boldsymbol{e}^{\mathcal{O}} \to 0$ as $t \to \infty$ (asymptotic stability). Note that $\boldsymbol{r}^{\mathcal{T}}_d$ is a time-varying quantity and its direction in space depends upon the attitude of the target.

B. Attitude Synchronization

An attitude error between the desired orientation of the pursuer's docking port and the current orientation is constructed, and the objective of the attitude controller is to find the torque input necessary to nullify this error. The desired orientation in this case is constructed as the mirror image of the target's docking port direction. Note that because the target is uncontrolled and tumbles freely, the direction of the docking port on the target changes as well; hence, the desired orientation of the pursuer's docking port changes as well.

IV. Control Law Derivation

The control law derivation is summarized in two parts. The first part deals with derivation of a translational control law that seeks to align the pursuer along the desired relative position vector while maintaining a safe separation distance. The second part deals with an attitude reorientation maneuver that orients the pursuer's docking port in the desired direction. *We reiterate that the separate derivations are merely to facilitate understanding the details. We do not require the translation or the attitude errors to converge in any particular order*. The details of the implementation of the control laws are summarized in Fig. 3.

A. Relative Position Tracking Control Law

As mentioned, the goal of this controller is to ensure that

$$\boldsymbol{e}^{\mathcal{O}} = \boldsymbol{r}^{\mathcal{O}} - [\boldsymbol{C}_{\mathcal{O}\mathcal{T}}]\boldsymbol{r}^{\mathcal{T}}_d \to 0$$

This ensures that the pursuer is aligned with the docking port of the target and that it is located at the desired relative distance from the target. Restricting our attention to derivation of the error quantities with respect to the LVLH frame and because

$$\boldsymbol{e}^{\mathcal{O}} = \boldsymbol{r}^{\mathcal{O}} - r_d[\boldsymbol{C}_{\mathcal{O}\mathcal{T}}]\hat{i}_{\mathcal{T}}$$

we obtain

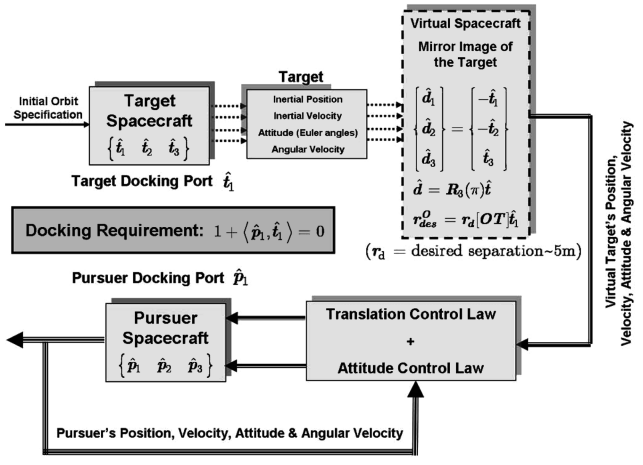

Fig. 3 Control algorithm implementation for pursuer–target cooperative docking.

$$\dot{\boldsymbol{e}}^{\mathcal{O}} = \dot{\boldsymbol{r}}^{\mathcal{O}} - r_d[\boldsymbol{C}_{\mathcal{OT}}]\left(\boldsymbol{\omega}^{\mathcal{T}}_{\mathcal{OT}} \times \hat{\imath}_{\mathcal{T}}\right) \tag{11}$$

Also,

$$\ddot{\boldsymbol{e}}^{\mathcal{O}} = \ddot{\boldsymbol{r}}^{\mathcal{O}} - r_d[\boldsymbol{C}_{\mathcal{OT}}]\left(\dot{\boldsymbol{\omega}}^{\mathcal{T}}_{\mathcal{OT}} \times \hat{\boldsymbol{\imath}}_{\mathcal{T}} + \boldsymbol{\omega}^{\mathcal{T}}_{\mathcal{OT}} \times \boldsymbol{\omega}^{\mathcal{T}}_{\mathcal{OT}} \times \hat{\boldsymbol{\imath}}_{\mathcal{T}}\right) \tag{12}$$

Note that $\boldsymbol{\omega}^{\mathcal{T}}_{\mathcal{OT}} = \boldsymbol{\omega}^{\mathcal{T}}_{\mathcal{NT}} - \boldsymbol{\omega}^{\mathcal{T}}_{\mathcal{NO}}$ and

$$\dot{\boldsymbol{\omega}}^{\mathcal{T}}_{\mathcal{OT}} = \dot{\boldsymbol{\omega}}^{\mathcal{T}}_{\mathcal{NT}} - \operatorname{skew}\left(\boldsymbol{\omega}^{\mathcal{T}}_{\mathcal{OT}}\right)[\boldsymbol{C}_{\mathcal{TO}}]\boldsymbol{\omega}^{\mathcal{O}}_{\mathcal{NO}} + [\boldsymbol{C}_{\mathcal{TO}}]\dot{\boldsymbol{\omega}}^{\mathcal{O}}_{\mathcal{NO}}\rho$$

We observe that $\dot{\boldsymbol{\omega}}^{\mathcal{T}}_{\mathcal{NT}}$ is obtained from Eq. (7) and $\dot{\boldsymbol{\omega}}^{\mathcal{O}}_{\mathcal{NO}}$ is obtained from the target's orbit evolution, and the formulation allows for a description of the generic orbit evolution in the presence of uncertainties that perturb the orbital elements.

In the absence of any perturbation forces on the target's orbit, $\dot{\boldsymbol{\omega}}^{\mathcal{O}}_{\mathcal{NO}}$ can also be described based on Eq. (5) and $\dot{\boldsymbol{\omega}}^{\mathcal{T}}_{\mathcal{OT}}$ can be expressed as

$$\begin{aligned}\dot{\boldsymbol{\omega}}^{\mathcal{T}}_{\mathcal{OT}} = {} & -\boldsymbol{H}_{\mathcal{T}}^{-1}\operatorname{skew}\left(\boldsymbol{\omega}^{\mathcal{T}}_{\mathcal{NT}}\right)\boldsymbol{H}_{\mathcal{T}}\boldsymbol{\omega}^{\mathcal{T}}_{\mathcal{NT}} + \boldsymbol{H}_{\mathcal{T}}^{-1}\boldsymbol{\delta}_{\mathcal{T}} \\ & - \operatorname{skew}\left(\boldsymbol{\omega}^{\mathcal{T}}_{\mathcal{OT}}\right)[\boldsymbol{C}_{\mathcal{TO}}]\boldsymbol{\omega}^{\mathcal{O}}_{\mathcal{NO}} + [\boldsymbol{C}_{\mathcal{TO}}]\begin{bmatrix} 0 & 0 & -2\frac{\dot{R}_{\mathcal{T}}}{R_{\mathcal{T}}}\boldsymbol{\omega}^{\mathcal{O}}_{\mathcal{NO}}(3,1)\end{bmatrix}^T\end{aligned} \tag{13}$$

$$\dot{\boldsymbol{\omega}}^{\mathcal{T}}_{\mathcal{OT}} = \boldsymbol{f}_0\left(\boldsymbol{C}_{\mathcal{TO}}, \boldsymbol{\omega}^{\mathcal{O}}_{\mathcal{NO}}, R_{\mathcal{T}}, \dot{R}_{\mathcal{T}}\right) + \boldsymbol{f}_h\left(\boldsymbol{\omega}^{\mathcal{T}}_{\mathcal{NT}}, \boldsymbol{H}_{\mathcal{T}}, \boldsymbol{\delta}_{\mathcal{T}}\right) \tag{14}$$

where $[\boldsymbol{C}_{\mathcal{TO}}] = [\boldsymbol{C}_{\mathcal{TN}}][\boldsymbol{C}_{\mathcal{NO}}]$. It is evident from Eq. (14) that the terms in $\boldsymbol{f}_h$ contain the target's inertia as well as the disturbance torques acting on the target. However, a linear representation of the unknown/uncertain parameters is possible, and this will be exploited in the adaptive control design.

The translational tracking-error dynamics can then be compactly expressed as

$$\begin{aligned}\ddot{\boldsymbol{e}}^{\mathcal{O}} = {} & \boldsymbol{A}_1\boldsymbol{r}^{\mathcal{O}} + \boldsymbol{A}_2\dot{\boldsymbol{r}}^{\mathcal{O}} - r_d[\boldsymbol{C}_{\mathcal{OT}}]\left(\dot{\boldsymbol{\omega}}^{\mathcal{T}}_{\mathcal{OT}} \times \hat{\boldsymbol{\imath}}_{\mathcal{T}} + \boldsymbol{\omega}^{\mathcal{T}}_{\mathcal{OT}}\right. \\ & \left. \times\, \boldsymbol{\omega}^{\mathcal{T}}_{\mathcal{OT}} \times \hat{\boldsymbol{\imath}}_{\mathcal{T}}\right) + \boldsymbol{u} + \boldsymbol{f}\end{aligned} \tag{15}$$

$$\begin{aligned}\ddot{\boldsymbol{e}}^{\mathcal{O}} = {} & \boldsymbol{A}_1\boldsymbol{r}^{\mathcal{O}} + \boldsymbol{A}_2\dot{\boldsymbol{r}}^{\mathcal{O}} - r_d[\boldsymbol{C}_{\mathcal{OT}}]\left(\boldsymbol{f}_0\left(\boldsymbol{C}_{\mathcal{TO}}, \boldsymbol{\omega}^{\mathcal{O}}_{\mathcal{NO}}, R_{\mathcal{T}}, \dot{R}_{\mathcal{T}}\right)\right. \\ & \left. \times\, \hat{\boldsymbol{\imath}}_{\mathcal{T}} + \boldsymbol{f}_h\left(\boldsymbol{\omega}^{\mathcal{T}}_{\mathcal{NT}}, \boldsymbol{H}_{\mathcal{T}}, \boldsymbol{\delta}_{\mathcal{T}}\right) \times \hat{\boldsymbol{\imath}}_{\mathcal{T}} + \boldsymbol{\omega}^{\mathcal{T}}_{\mathcal{OT}} \times \boldsymbol{\omega}^{\mathcal{T}}_{\mathcal{OT}} \times \hat{\boldsymbol{\imath}}_{\mathcal{T}}\right) + \boldsymbol{u} + \boldsymbol{f}\end{aligned} \tag{16}$$

where

$$\boldsymbol{A}_1 = \begin{bmatrix} \dot{\theta}^2 + \frac{2\mu}{R_{\mathcal{T}}^3} & \ddot{\theta} & 0 \\ -\ddot{\theta} & \dot{\theta}^2 - \frac{\mu}{R_{\mathcal{T}}^3} & 0 \\ 0 & 0 & -\frac{\mu}{R_{\mathcal{T}}^3} \end{bmatrix}$$

and

$$\boldsymbol{A}_2 = \begin{bmatrix} 0 & 2\dot{\theta} & 0 \\ -2\dot{\theta} & 0 & 0 \\ 0 & 0 & 0 \end{bmatrix}$$

The synthesis of the controller follows a feedback-linearization-like approach [10–13] and is detailed next.

A control law that consists of a proportional–integral–derivative type of structure with the feedback terms associated with

$$\boldsymbol{e}^{\mathcal{O}} \qquad \int_0^t \boldsymbol{e}^{\mathcal{O}}(s)\,\mathrm{d}s \qquad \dot{\boldsymbol{e}}^{\mathcal{O}}$$

and a nonlinear function

$$\boldsymbol{f}_c\left(\boldsymbol{r}^{\mathcal{O}}, \dot{\boldsymbol{r}}^{\mathcal{O}}, \boldsymbol{\omega}^{\mathcal{T}}_{\mathcal{OT}}, \dot{\boldsymbol{\omega}}^{\mathcal{T}}_{\mathcal{OT}}, \hat{\imath}_{\mathcal{T}}\right)$$

that is yet to be determined is proposed to meet the desired control objective:

$$\begin{aligned}\boldsymbol{u} = {} & -\boldsymbol{K}P\boldsymbol{e}^{\mathcal{O}} - \boldsymbol{K}_D\dot{\boldsymbol{e}}^{\mathcal{O}} - \boldsymbol{K}_I\int_0^t \boldsymbol{e}^{\mathcal{O}}(s)\,\mathrm{d}s \\ & + \boldsymbol{f}_c\left(\boldsymbol{r}^{\mathcal{O}}, \dot{\boldsymbol{r}}^{\mathcal{O}}, \boldsymbol{\omega}^{\mathcal{T}}_{\mathcal{OT}}, \dot{\boldsymbol{\omega}}^{\mathcal{T}}_{\mathcal{OT}}, \hat{\imath}_{\mathcal{T}}\right)\end{aligned} \tag{17}$$

where $\boldsymbol{K}_P$, $\boldsymbol{K}_D$, and $\boldsymbol{K}_I \in \mathbb{R}^{3\times 3}$ are positive-definite diagonal matrices corresponding to the proportional, derivative, and integral matrix feedback gains, respectively.

Theorem 1. For the case when all external disturbances are absent, the transitional control law specified in Eq. (17) asymptotically stabilizes the translational dynamics governed by Eq. (15): that is, $(\boldsymbol{e}, \dot{\boldsymbol{e}}) \to 0$ as $t \to \infty$.

Proof. Setting the disturbances to zero and substituting the control law from Eq. (17) into Eq. (16), we obtain

$$\begin{aligned}& \ddot{\boldsymbol{e}}^{\mathcal{O}} + \boldsymbol{K}_D\dot{\boldsymbol{e}}^{\mathcal{O}} + \boldsymbol{K}_P\boldsymbol{e}^{\mathcal{O}} + \boldsymbol{K}_I\int_0^t \boldsymbol{e}^{\mathcal{O}}(s)\,\mathrm{d}s \\ & \quad = \boldsymbol{f}_c\left(\boldsymbol{r}^{\mathcal{O}}, \dot{\boldsymbol{r}}^{\mathcal{O}}, \boldsymbol{\omega}^{\mathcal{T}}_{\mathcal{OT}}, \dot{\boldsymbol{\omega}}^{\mathcal{T}}_{\mathcal{OT}}, \hat{\imath}_{\mathcal{T}}\right) + \boldsymbol{A}_1\boldsymbol{r}^{\mathcal{O}} + \boldsymbol{A}_2\dot{\boldsymbol{r}}^{\mathcal{O}} \\ & \quad - r_d[\boldsymbol{C}_{\mathcal{OT}}]\boldsymbol{f}_0\left(\boldsymbol{C}_{\mathcal{TO}}, \boldsymbol{\omega}^{\mathcal{O}}_{\mathcal{NO}}, R_{\mathcal{T}}, \dot{R}_{\mathcal{T}}\right) \\ & \quad \times \hat{\boldsymbol{\imath}}_{\mathcal{T}} - r_d[\boldsymbol{C}_{\mathcal{OT}}]\boldsymbol{H}_{\mathcal{T}}^{-1}\operatorname{skew}\left(\boldsymbol{\omega}^{\mathcal{T}}_{\mathcal{NT}}\right)\boldsymbol{H}_{\mathcal{T}}\boldsymbol{\omega}^{\mathcal{T}}_{\mathcal{NT}} \times \hat{\boldsymbol{\imath}}_{\mathcal{T}}\end{aligned}$$

Also, the right-hand side (RHS) of the preceding equation can be further simplified as

$$\begin{aligned}\mathrm{RHS} = {} & \boldsymbol{f}_c\left(\boldsymbol{r}^{\mathcal{O}}, \dot{\boldsymbol{r}}^{\mathcal{O}}, \boldsymbol{\omega}^{\mathcal{T}}_{\mathcal{OT}}, \dot{\boldsymbol{\omega}}^{\mathcal{T}}_{\mathcal{OT}}, \hat{\imath}_{\mathcal{T}}\right) + \boldsymbol{A}_1\boldsymbol{r}^{\mathcal{O}} \\ & + \boldsymbol{A}_2\dot{\boldsymbol{r}}^{\mathcal{O}} - r_d[\boldsymbol{C}_{\mathcal{OT}}]\boldsymbol{f}_0\left(\boldsymbol{C}_{\mathcal{TO}}, \boldsymbol{\omega}^{\mathcal{O}}_{\mathcal{NO}}, R_{\mathcal{T}}, \dot{R}_{\mathcal{T}}\right) \\ & \times \hat{\boldsymbol{\imath}}_{\mathcal{T}} - r_d[\boldsymbol{C}_{\mathcal{OT}}]\boldsymbol{L}^*\boldsymbol{g} \times \hat{\boldsymbol{\imath}}_{\mathcal{T}}\end{aligned}$$

where $\boldsymbol{L}^* \in \mathbb{R}^{3\times 6}$ and $\boldsymbol{g} \in \mathbb{R}^{6\times 1}$. Further we recognize that

$$\operatorname{skew}\left(\boldsymbol{\omega}^{\mathcal{T}}_{\mathcal{NT}}\right)\boldsymbol{H}_{\mathcal{T}}\boldsymbol{\omega}^{\mathcal{T}}_{\mathcal{NT}} = \boldsymbol{L}_1\boldsymbol{g}$$

The definitions of $\boldsymbol{L}_1$ and $\boldsymbol{g}$ follow from [14,15]. We thus conclude that $\boldsymbol{L}^* = \boldsymbol{H}_{\mathcal{T}}^{-1}\boldsymbol{L}_1$. For the case when all parameters (i.e., target inertia) are known exactly, a specific choice of

$$\boldsymbol{f}_c\left(\boldsymbol{r}^{\mathcal{O}}, \dot{\boldsymbol{r}}^{\mathcal{O}}, \boldsymbol{\omega}^{\mathcal{T}}_{\mathcal{OT}}, \dot{\boldsymbol{\omega}}^{\mathcal{T}}_{\mathcal{OT}}, \hat{\imath}_{\mathcal{T}}\right)$$

that ensures asymptotically stable translational error dynamics is

$$\begin{aligned}\boldsymbol{f}_c\left(\boldsymbol{r}^{\mathcal{O}}, \dot{\boldsymbol{r}}^{\mathcal{O}}, \boldsymbol{\omega}^{\mathcal{T}}_{\mathcal{OT}}, \dot{\boldsymbol{\omega}}^{\mathcal{T}}_{\mathcal{OT}}, \hat{\imath}_{\mathcal{T}}\right) = {} & -\boldsymbol{A}_1\boldsymbol{r}^{\mathcal{O}} - \boldsymbol{A}_2\dot{\boldsymbol{r}}^{\mathcal{O}} \\ & + r_d[\boldsymbol{C}_{\mathcal{OT}}]\boldsymbol{f}_0\left(\boldsymbol{C}_{\mathcal{TO}}, \boldsymbol{\omega}^{\mathcal{O}}_{\mathcal{NO}}, R_{\mathcal{T}}, \dot{R}_{\mathcal{T}}\right) \times \hat{\boldsymbol{\imath}}_{\mathcal{T}} + r_d[\boldsymbol{C}_{\mathcal{OT}}]\boldsymbol{L}^*\boldsymbol{g} \times \hat{\boldsymbol{\imath}}_{\mathcal{T}}\end{aligned}$$

For this choice of $\boldsymbol{f}_c(\cdots)$, the closed-loop translation error dynamics reduce to

$$\ddot{\boldsymbol{e}}^{\mathcal{O}} + \boldsymbol{K}_D\dot{\boldsymbol{e}}^{\mathcal{O}} + \boldsymbol{K}_P\boldsymbol{e}^{\mathcal{O}} + \boldsymbol{K}_I\int_0^t \boldsymbol{e}^{\mathcal{O}}(s)\,\mathrm{d}s = 0$$

which is rendered uniformly exponentially stable for an appropriate choice of $\{\boldsymbol{K}_P\boldsymbol{K}_I\boldsymbol{K}_D\}$. In this case, these gains should be chosen such that $\boldsymbol{K}_P, \boldsymbol{K}_D, \boldsymbol{K}_I > 0$ and $\boldsymbol{K}_P - \boldsymbol{K}_D^{-1}\boldsymbol{K}_I > 0$.

However, because the target inertia parameters are not known a priori, the aforementioned control law with the choice of $\boldsymbol{f}_c(\cdots)$ as previously specified cannot be implemented. Reference [2] suggests a method to estimate the inertia parameters based on radar images. In this paper, to remedy this an online estimate of the parameter matrix $\boldsymbol{L}^*$ given by $\boldsymbol{L}(t)$ is synthesized. The nonlinear function $\boldsymbol{f}_c(\cdots)$ is then specified as

$$\boldsymbol{f}_c\left(\boldsymbol{r}^{\mathcal{O}}, \dot{\boldsymbol{r}}^{\mathcal{O}}, \boldsymbol{\omega}_{\mathcal{OT}}^{\mathcal{T}}, \dot{\boldsymbol{\omega}}_{\mathcal{OT}}^{\mathcal{T}}, \hat{\boldsymbol{i}}_T\right) = -\boldsymbol{A}_1\boldsymbol{r}^{\mathcal{O}} - \boldsymbol{A}_2\dot{\boldsymbol{r}}^{\mathcal{O}} + r_d[\boldsymbol{C}_{\mathcal{OT}}]\boldsymbol{f}_0\left(\boldsymbol{C}_{\mathcal{TO}}, \boldsymbol{\omega}_{\mathcal{NO}}^{\mathcal{O}}, R_T, \dot{R}_T\right) \times \hat{\boldsymbol{i}}_T + r_d[\boldsymbol{C}_{\mathcal{OT}}]\boldsymbol{L}(t)\boldsymbol{g} \times \hat{\boldsymbol{i}}_T \tag{18}$$

Using this definition of $\boldsymbol{f}_c(\ldots)$ from Eq. (18), we now obtain the closed-loop translational error dynamics as

$$\ddot{\boldsymbol{e}}^{\mathcal{O}} + \boldsymbol{K}_D\dot{\boldsymbol{e}}^{\mathcal{O}} + \boldsymbol{K}_P\boldsymbol{e}^{\mathcal{O}} + \boldsymbol{K}_I\int_0^t \boldsymbol{e}^{\mathcal{O}}(s)\,\mathrm{d}s = r_d[\boldsymbol{C}_{\mathcal{OT}}]\tilde{\boldsymbol{L}}(t)\boldsymbol{g} \times \hat{\boldsymbol{i}}_T \tag{19}$$

where $\tilde{\boldsymbol{L}}(t) = \boldsymbol{L}(t) - \boldsymbol{L}^*$. The closed-loop dynamics in Eq. (19) can be rewritten using

$$\boldsymbol{z} = \begin{bmatrix} \int_0^t \boldsymbol{e}^{\mathcal{O}}(s)\,\mathrm{d}s & \boldsymbol{e}^{\mathcal{O}} & \dot{\boldsymbol{e}}^{\mathcal{O}} \end{bmatrix}^T$$

as

$$\dot{\boldsymbol{z}} = \boldsymbol{A}_c\boldsymbol{z} + \boldsymbol{B}_c\boldsymbol{\xi} \tag{20}$$

where $\boldsymbol{\xi} = -r_d\,\mathrm{skew}(\hat{\boldsymbol{i}}_T)[\boldsymbol{C}_{\mathcal{OT}}]\tilde{\boldsymbol{L}}(t)\boldsymbol{g}$,

$$\boldsymbol{A}_c = \begin{bmatrix} 0_{3\times3} & I_{3\times3} & 0_{3\times3} \\ 0_{3\times3} & 0_{3\times3} & I_{3\times3} \\ -\boldsymbol{K}_I & -\boldsymbol{K}_P & -\boldsymbol{K}_D \end{bmatrix} \quad \text{and} \quad \boldsymbol{B}_c = \begin{bmatrix} 0_{3\times3} \\ 0_{3\times3} \\ I_{3\times3} \end{bmatrix}$$

We note that the matrix $\boldsymbol{A}_c$ is Hurwitz (all eigenvalues have negative real parts). To show asymptotic stability of the closed-loop dynamics in Eq. (20), we begin with a candidate Lyapunov function and follow along the same lines described in [12]:

$$V = \tfrac{1}{2}\boldsymbol{z}^T\boldsymbol{P}_T\boldsymbol{z} + \tfrac{1}{2}r_d\,\mathrm{tr}\left(\tilde{\boldsymbol{L}}^T\Gamma_T^{-1}\tilde{\boldsymbol{L}}\right) \tag{21}$$

where $\Gamma_T = \Gamma_T^T > 0$ is a symmetric positive-definite adaptation gain matrix, and $\boldsymbol{P}_T = \boldsymbol{P}_T^T > 0$ is the symmetric positive-definite solution to the Lyapunov equation for a specified symmetric positive-definite matrix $\boldsymbol{Q}_T = \boldsymbol{Q}_T^T > 0$; that is,

$$\boldsymbol{P}_T\boldsymbol{A}_c + \boldsymbol{A}_c^T\boldsymbol{P}_T = -\boldsymbol{Q}_T$$

The solution $\boldsymbol{P}_T$ exists because $\boldsymbol{A}_c$ is Hurwitz.

Differentiating Eq. (21) along the trajectories in Eq. (20) and using the Lyapunov equation, we obtain

$$\frac{\mathrm{d}V}{\mathrm{d}t} = -\frac{1}{2}\boldsymbol{z}^T\boldsymbol{Q}_T\boldsymbol{z} + \boldsymbol{z}^T\boldsymbol{P}_T\boldsymbol{B}_c\boldsymbol{\xi} + r_d\,\mathrm{tr}\left(\tilde{\boldsymbol{L}}^T\Gamma_T^{-1}\dot{\tilde{\boldsymbol{L}}}\right) \tag{22}$$

The second term in Eq. (22) can be manipulated by making use of the trace identities from [16]. After a few manipulations, we obtain

$$\frac{\mathrm{d}V}{\mathrm{d}t} = -\frac{1}{2}\boldsymbol{z}^T\boldsymbol{Q}_T\boldsymbol{z} + r_d\,\mathrm{tr}\left(\tilde{\boldsymbol{L}}^T[\boldsymbol{C}_{\mathcal{OT}}]^T\,\mathrm{skew}(\hat{\boldsymbol{i}}_T)\boldsymbol{B}_c^T\boldsymbol{P}_T\boldsymbol{z}\boldsymbol{g}^T + \tilde{\boldsymbol{L}}^T\Gamma_T^{-1}\dot{\tilde{\boldsymbol{L}}}\right) \tag{23}$$

We choose the adaptive update law for $\dot{\boldsymbol{L}}(=\dot{\tilde{\boldsymbol{L}}})$ as

$$\dot{\boldsymbol{L}} = -\Gamma_T[\boldsymbol{C}_{\mathcal{OT}}]^T\,\mathrm{skew}(\hat{\boldsymbol{i}}_T)\boldsymbol{B}_c^T\boldsymbol{P}_T\boldsymbol{z}\boldsymbol{g}^T \qquad \text{since } \boldsymbol{L}^* = \text{const} \tag{24}$$

With the choice of the adaptation law as in Eq. (23), Eq. (24) reduces to

$$\frac{\mathrm{d}V}{\mathrm{d}t} = -\frac{1}{2}\boldsymbol{z}^T\boldsymbol{Q}_T\boldsymbol{z} \le 0 \tag{25}$$

Because $V > 0$ and $\mathrm{d}V/\mathrm{d}t \le 0$, we conclude that $\boldsymbol{z},\ \tilde{\boldsymbol{L}} \in \mathcal{L}_\infty$. Further, integrating Eq. (25) from 0 to ∞, it can be trivially shown that $\boldsymbol{z} \in \mathcal{L}_2$; thus, $\boldsymbol{z} \in \mathcal{L}_2 \cap \mathcal{L}_\infty$. To prove asymptotic stability of the translational error dynamics, it needs to be shown that $\dot{\boldsymbol{z}} \in \mathcal{L}_\infty$. Looking at the expression for $\boldsymbol{\xi}$, the boundedness of $\boldsymbol{\xi}$ is guaranteed as long as $\boldsymbol{g}$ is bounded. Recall that $\boldsymbol{g}$ is composed of the components of the angular velocity of the target satellite. *If there are no external disturbance torques on the target satellite, then the target's rotational kinetic energy remains constant. However, this cannot be guaranteed for an uncontrolled satellite experiencing significant disturbances. In essence, this is also the primary challenge with the synchronization-based capture of an uncontrolled satellite subject to disturbing forces and torques*. Therefore, from Barbalat's lemma [17], we conclude that $\boldsymbol{z} \to 0$ as $t \to \infty$. In other words, $\boldsymbol{r}^{\mathcal{O}} \to r_d[\boldsymbol{C}_{\mathcal{OT}}]\hat{\boldsymbol{i}}_T$ as $t \to \infty$. □

For the problem under consideration, the natural perturbing forces due to differential gravity, solar radiation pressure, and differential atmospheric drag are very small and are treated to be constant disturbance forces. The integral action is introduced into the control law to counter these disturbances [18]. In the presence of unknown yet bounded disturbances (i.e., $\|\boldsymbol{f}\|_\infty \le f_m$), it is possible to robustify the adaptive laws further to show the convergence of the tracking errors to a residual set. In this context, when bounded unknown disturbances are present, the robust adaptation law [17] (namely, the ν modification) is given as follows:

$$\dot{\boldsymbol{L}} = -\Gamma_T[\boldsymbol{C}_{\mathcal{OT}}]^T\,\mathrm{skew}(\hat{\boldsymbol{i}}_T)\boldsymbol{B}_c^T\boldsymbol{P}_T\boldsymbol{z}\boldsymbol{g}^T - \nu\boldsymbol{L} \tag{26}$$

for some $\nu > 0$. The time derivative of the Lyapunov function candidate is then obtained as

$$\frac{\mathrm{d}V}{\mathrm{d}t} = -\frac{1}{2}\boldsymbol{z}^T\boldsymbol{Q}_T\boldsymbol{z} + \boldsymbol{z}^T\boldsymbol{P}_T\boldsymbol{B}_c\boldsymbol{f} - \nu r_d\,\mathrm{tr}\left(\tilde{\boldsymbol{L}}^T\Gamma_T^{-1}\boldsymbol{L}\right) \tag{27}$$

Now, using straightforward completion of squares [or even Young's inequality on the second term of the RHS of Eq. (27)], it can be shown that

$$\frac{\mathrm{d}V}{\mathrm{d}t} \le -\frac{1}{2}\boldsymbol{z}^T\left[\boldsymbol{Q}_T - \alpha_0^{-1}\boldsymbol{I}\right]\boldsymbol{z} + \frac{\alpha_0}{2}\|\boldsymbol{P}_T\boldsymbol{B}_c f_m\|^2 - \nu r_d\,\mathrm{tr}\left(\tilde{\boldsymbol{L}}^T\Gamma_T^{-1}\boldsymbol{L}\right) \tag{28}$$

for some $\alpha_0 > 0$. Further,

$$\begin{aligned}\dot{V} &\le -\frac{1}{2}\boldsymbol{z}^T[\boldsymbol{Q}_T - \alpha_0^{-1}\boldsymbol{I}]\boldsymbol{z} - \frac{\nu}{2}r_d\,\mathrm{tr}(\tilde{\boldsymbol{L}}^T\Gamma_T^{-1}\tilde{\boldsymbol{L}}) \\ &\quad + \frac{\alpha_0}{2}\|\boldsymbol{P}_T\boldsymbol{B}_c f_m\|^2 + \frac{\nu}{2}r_d\,\mathrm{tr}(\boldsymbol{L}^{*T}\Gamma_T^{-1}\boldsymbol{L}^*) \\ &\le -\gamma V - \frac{1}{2}\boldsymbol{z}^T[\boldsymbol{Q}_T - \alpha_0^{-1}\boldsymbol{I} - 2\gamma\boldsymbol{P}_T]\boldsymbol{z} \\ &\quad - \left(\frac{\nu}{2} - \gamma\right)r_d\,\mathrm{tr}(\tilde{\boldsymbol{L}}^T\Gamma_T^{-1}\tilde{\boldsymbol{L}}) + \frac{\nu}{2}r_d\,\mathrm{tr}(\boldsymbol{L}^{*T}\Gamma_T^{-1}\boldsymbol{L}^*) + \frac{\alpha_0}{2}\|\boldsymbol{P}_T\boldsymbol{B}_c f_m\|^2\end{aligned}$$

Choosing

$$\gamma = \min\left[\frac{1}{2}\mu\left(\boldsymbol{Q}_T - \alpha_0^{-1}\boldsymbol{I}\right)\mu\left(\boldsymbol{P}_T^{-1}\right), \frac{\nu}{2}\right]$$

where $\mu(\cdot)$ is the spectral radius operator [19,20], it follows that

$$\dot{V} \le -\gamma V + \frac{\nu}{2}r_d\,\mathrm{tr}\left(\boldsymbol{L}^{*T}\Gamma_T^{-1}\boldsymbol{L}^*\right) + \frac{\alpha_0\|\boldsymbol{P}_T\boldsymbol{B}_c\boldsymbol{f}\|^2}{2} \tag{29}$$

Thus, $\dot{V} \le 0$ whenever

$$V \ge V_0 \triangleq \frac{1}{\gamma}\left[\frac{\nu}{2}r_d\,\mathrm{tr}\left(\boldsymbol{L}^{*T}\Gamma_T^{-1}\boldsymbol{L}^*\right) + \frac{\alpha_0\|\boldsymbol{P}_T\boldsymbol{B}_c f_m\|^2}{2}\right] \tag{30}$$

Thus, with the ν modification, we extend the properties of the adaptive laws for the no-disturbance case to the nonideal case when disturbances are present. A drawback of this technique, however, is that the L_2 property of $\boldsymbol{z}$ is no longer guaranteed in the presence of the nonzero disturbance term $\boldsymbol{f}$. However, $\boldsymbol{z}$ can be shown to be $f_m^2 + \nu$ small in the mean square sense. This could lead to an undesirable phenomenon known as bursting and can be avoided by using a different robustification scheme such as the dead-zone modification (see [17] for more details).

Also note that for the case when the external disturbances are constant, the control law could be trivially modified to include a feedforward term; that is

$$\boldsymbol{u} = -\hat{\boldsymbol{f}} - \boldsymbol{K}_P \boldsymbol{e}^{\mathcal{O}} - \boldsymbol{K}_D \dot{\boldsymbol{e}}^{\mathcal{O}} - \boldsymbol{K}_I \int_0^t \boldsymbol{e}^{\mathcal{O}}(s)\,\mathrm{d}s + \boldsymbol{f}_c(\cdots)$$

where $\hat{\boldsymbol{f}}(t)$ is the feedforward estimate of the unknown constant disturbance $\boldsymbol{f}$. With this choice of the control law, the closed-loop error dynamics become

$$\dot{\boldsymbol{z}} = \boldsymbol{A}_c \boldsymbol{z} + \boldsymbol{B}_c \boldsymbol{\xi} + \boldsymbol{B}_c \tilde{\boldsymbol{f}} \tag{31}$$

where $\tilde{\boldsymbol{f}} = \boldsymbol{f} - \hat{\boldsymbol{f}}$. We then choose a Lyapunov function candidate

$$V = \frac{1}{2}\boldsymbol{z}^T \boldsymbol{P}_T \boldsymbol{z} + \frac{1}{2} r_d \,\mathrm{tr}\left(\tilde{\boldsymbol{L}}^T \Gamma_T^{-1} \tilde{\boldsymbol{L}}\right) + \frac{1}{\beta}\tilde{\boldsymbol{f}}^T \tilde{\boldsymbol{f}}$$

where $\beta > 0$. On differentiating V with respect to time and evaluating the trajectories along the closed-loop error dynamics, substituting the adaptive laws for $\boldsymbol{L}$ as in Eq. (24), we obtain

$$\dot{V} = -\frac{1}{2}\boldsymbol{z}^T \boldsymbol{Q}_T \boldsymbol{z} + \boldsymbol{z}^T \boldsymbol{P}_T \boldsymbol{B}_c \tilde{\boldsymbol{f}} + \frac{1}{\beta}\dot{\tilde{\boldsymbol{f}}}^T \tilde{\boldsymbol{f}}$$

Thus, the estimate of the feedforward disturbance cancellation term is simply

$$\dot{\tilde{\boldsymbol{f}}} = -\dot{\hat{\boldsymbol{f}}} = -\beta \boldsymbol{B}_c^T \boldsymbol{P}_T \boldsymbol{z}$$

or

$$\dot{\hat{\boldsymbol{f}}} = \beta \boldsymbol{B}_c^T \boldsymbol{P}_T \boldsymbol{z}$$

The proof of asymptotic stability of the translational error dynamics thereafter follows along the same lines as that described earlier. It should be noted that had the control law been prescribed to be of a proportional–derivative kind, the feedforward estimate of the constant disturbance would essentially have involved the integral of the translational error, thereby introducing the integral feedback term.

B. Attitude-Synchronization Control Law

Although the control law derived earlier maneuvers the pursuer satellite to align with a specific desired position vector, an additional maneuver is performed simultaneously that reorients the pursuer satellite so that the docking port of the pursuer faces the docking port on the target satellite. To begin the control law derivation for this maneuver, the rotational kinematics and the Euler equations representing the attitude dynamics of the pursuer are combined to provide a more convenient representation of the rotational equations of motion. After some algebraic manipulation, the rotational equations of motion of the purser can be expressed by the following equation [21,22]:

$$\boldsymbol{H}_{\mathcal{P}}^*(\boldsymbol{\sigma}_{\mathcal{P}})\ddot{\boldsymbol{\sigma}}_{\mathcal{P}} + \boldsymbol{C}_{\mathcal{P}}^*(\boldsymbol{\sigma}_{\mathcal{P}}, \dot{\boldsymbol{\sigma}}_{\mathcal{P}})\dot{\boldsymbol{\sigma}}_{\mathcal{P}} = \bar{\boldsymbol{\tau}}_{\mathcal{P}} + \bar{\boldsymbol{\delta}}_{\mathcal{P}} \tag{32}$$

where

$$\boldsymbol{J}_{\mathcal{P}} = \left[\left(1 - \boldsymbol{\sigma}_{\mathcal{P}}^T \boldsymbol{\sigma}_{\mathcal{P}}\right) I_{3\times 3} + 2[\tilde{\boldsymbol{\sigma}}_{\mathcal{P}}] + 2\boldsymbol{\sigma}_{\mathcal{P}} \boldsymbol{\sigma}_{\mathcal{P}}^T\right] \qquad \boldsymbol{J}_{\mathcal{P}}^{-T} = \left[\boldsymbol{J}_{\mathcal{P}}^{-1}\right]^T$$

$$\boldsymbol{H}_{\mathcal{P}}^*(\boldsymbol{\sigma}_{\mathcal{P}}) = 4\boldsymbol{J}_{\mathcal{P}}^{-T} \boldsymbol{H}_{\mathcal{P}} \boldsymbol{J}_{\mathcal{P}}^{-1}$$

$$\boldsymbol{C}_{\mathcal{P}}^*(\boldsymbol{\sigma}_{\mathcal{P}}, \dot{\boldsymbol{\sigma}}_{\mathcal{P}}) = -4\left(\boldsymbol{H}_{\mathcal{P}}^*(\boldsymbol{\sigma}_{\mathcal{P}})\frac{\mathrm{d}}{\mathrm{d}t}(\boldsymbol{J}_{\mathcal{P}})\boldsymbol{J}_{\mathcal{P}}^{-1} + \boldsymbol{J}_{\mathcal{P}}^{-T}\mathrm{skew}(\boldsymbol{H}_{\mathcal{P}}\boldsymbol{J}_{\mathcal{P}}^{-1}\dot{\boldsymbol{\sigma}}_{\mathcal{P}})\boldsymbol{J}_{\mathcal{P}}^{-1}\right)$$

$$\bar{\boldsymbol{\delta}}_{\mathcal{P}} = \boldsymbol{J}_{\mathcal{P}}^{-T}\boldsymbol{\delta}_{\mathcal{P}} \qquad \bar{\boldsymbol{\tau}}_{\mathcal{P}} = \boldsymbol{J}_{\mathcal{P}}^{-T}\boldsymbol{\tau}_{\mathcal{P}}$$

The symmetry of the moment-of-intertia matrix $\boldsymbol{H}_{\mathcal{P}}$ can be exploited so that the gravity gradient disturbance model can be parameterized with respect to the vector containing the six different components that make up $\boldsymbol{H}_{\mathcal{P}}$.

This inertia vector is given by

$$\boldsymbol{\theta}_{\mathcal{P}}^* = [\,\boldsymbol{H}_{\mathcal{P}(1,1)} \quad \boldsymbol{H}_{\mathcal{P}(2,2)} \quad \boldsymbol{H}_{\mathcal{P}(3,3)} \quad \boldsymbol{H}_{\mathcal{P}(1,2)} \quad \boldsymbol{H}_{\mathcal{P}(1,3)} \quad \boldsymbol{H}_{\mathcal{P}(2,3)}\,]^T$$

and following the approach outlined in [21,23], we note that given $\boldsymbol{\nu} = [\,\nu_1 \quad \nu_2 \quad \nu_3\,]^T$, the following relationship holds true:

$$\boldsymbol{H}_{\mathcal{P}}\boldsymbol{\nu} = \boldsymbol{\Lambda}(\boldsymbol{\nu})\boldsymbol{\theta}_{\mathcal{P}}^* \tag{33}$$

where the operator $\boldsymbol{\Lambda}(\boldsymbol{\nu})$ is defined by

$$\boldsymbol{\Lambda}(\boldsymbol{\nu}) \equiv \begin{bmatrix} \nu_1 & 0 & 0 & \nu_2 & \nu_3 & 0 \\ 0 & \nu_2 & 0 & \nu_1 & 0 & \nu_3 \\ 0 & 0 & \nu_3 & 0 & \nu_1 & \nu_2 \end{bmatrix}$$

Given this relationship, the net external disturbance torque acting on the pursuer, as listed in Eq. (10), can be modeled in the following form:

$$\bar{\boldsymbol{\delta}}_{\mathcal{P}} = \boldsymbol{J}_{\mathcal{P}}^{-T}\left(\boldsymbol{Y}\boldsymbol{\theta}_{\mathcal{P}}^* + \boldsymbol{\Psi}\boldsymbol{\delta}_{\mathcal{P}}^*\right) \tag{34}$$

where the matrix $\boldsymbol{Y} \in \mathbb{R}^{3\times 6}$ and $\boldsymbol{\Psi} \in \mathbb{R}^{3\times 9}$ are given by

$$\boldsymbol{Y} = -\frac{\mu}{R_{\mathcal{P}}^5}\,\mathrm{skew}\left(\boldsymbol{R}_{\mathcal{P}}^{\mathcal{P}}\right)\boldsymbol{\Lambda}\left(\boldsymbol{R}_{\mathcal{P}}^{\mathcal{P}}\right)$$

$$\boldsymbol{\Psi} = [\,I_{3\times 3} \quad \cos(\lambda t) I_{3\times 3} \quad \sin(\lambda t) I_{3\times 3}\,]$$

and

$$\boldsymbol{\delta}_{\mathcal{P}}^* = \begin{pmatrix} \boldsymbol{\delta}_{\mathcal{P}0} \\ \boldsymbol{\delta}_{\mathcal{P}c} \\ \boldsymbol{\delta}_{\mathcal{P}s} \end{pmatrix}$$

To synthesize the attitude control law, we define a desired attitude vector that the pursuer should track to achieve the control objective. The error associated with the orientation of the pursuer is then defined as $\boldsymbol{\varepsilon} = \boldsymbol{\sigma}_{\mathcal{P}} - \boldsymbol{\sigma}_{\mathcal{D}}$, where $\boldsymbol{\sigma}_{\mathcal{D}}$ is the desired orientation that ensures the docking port vector points in the direction exactly opposite that of the receiving port on the target. Because the translational control law ensures that the pursuer is at the desired relative distance directed along the outward normal from the receiving port, the pursuer now needs to perform the reorientation maneuver for synchronization: that is, $1 + \cos\langle \hat{\boldsymbol{d}}_{\mathcal{P}}, \hat{\boldsymbol{d}}_{\mathcal{T}} \rangle = 0$. Hence, to complete the reorientation of the pursuer to align $\hat{\boldsymbol{d}}_{\mathcal{P}} (= \hat{i}_{\mathcal{P}})$ along $-\hat{\boldsymbol{d}}_{\mathcal{T}} (= -\hat{i}_{\mathcal{T}})$, the following approach is proposed. We construct a "virtual desired reference frame" $\boldsymbol{C}_{\mathcal{DN}}$ that facilitates the preceding. Because the pursuer's docking port must always face the target's docking port, this is set up as follows:

$$\boldsymbol{C}_{\mathcal{DN}} = \mathcal{R}_1(0)\mathcal{R}_2(0)\mathcal{R}_3(\pi)\boldsymbol{C}_{\mathcal{TN}} \qquad \omega_{\mathcal{ND}}^{\mathcal{D}} = \boldsymbol{C}_{\mathcal{DN}}\boldsymbol{C}_{\mathcal{TN}}^T \omega_{\mathcal{NT}}^{\mathcal{T}}$$

where $\mathcal{R}_i(\alpha)$ corresponds to the unit rotation matrix about the ith axis through an angle α. The desired attitude, denoted as $\boldsymbol{\sigma}_{\mathcal{D}}$ (parameterized in terms of the MRPs), is then obtained from the principal rotation vector and the principal rotation angle computed from the direction cosine matrix $[\boldsymbol{C}_{\mathcal{ND}}]$, as shown in [7]. As mentioned earlier, the orientation error is defined as $\boldsymbol{\varepsilon} = \boldsymbol{\sigma}_{\mathcal{P}} - \boldsymbol{\sigma}_{\mathcal{D}}$, and the objective of the controller is to ensure that $\boldsymbol{\varepsilon} \to 0$ as $t \to \infty$. The derivation of the controller is outlined next.

The following closed-loop error dynamics are prescribed hence:

$$\boldsymbol{H}_{\mathcal{P}}^*\ddot{\boldsymbol{\varepsilon}} + \left(\bar{\boldsymbol{K}}_D + \boldsymbol{C}_{\mathcal{P}}^*\right)\dot{\boldsymbol{\varepsilon}} + \bar{\boldsymbol{K}}_P\boldsymbol{\varepsilon} = 0 \tag{35}$$

where $\bar{\boldsymbol{K}}_D$ and $\bar{\boldsymbol{D}}_P$ are positive-definite diagonal gain matrices, and $\boldsymbol{H}_{\mathcal{P}}^*$ is a symmetric positive-definite matrix. It can be shown that the aforementioned tracking-error dynamics are asymptotically stable [22]. To derive the attitude control law, the dynamics of the pursuer are substituted into the tracking-error dynamics to obtain

$$\bar{\boldsymbol{\tau}} = -\bar{\boldsymbol{K}}_P\boldsymbol{\varepsilon} - \bar{\boldsymbol{K}}_D\dot{\boldsymbol{\varepsilon}} - \boldsymbol{J}_{\mathcal{P}}^{-T}\left(\boldsymbol{Y}\boldsymbol{\theta}_{\mathcal{P}}^{*} + \boldsymbol{\Psi}\boldsymbol{\delta}_{\mathcal{P}}^{*}\right) \tag{36}$$

Because, in reality, the inertia parameters and the disturbance amplitudes are not exactly known, online estimates of these parameters are generated and used in the control law (following from the certainty equivalence principle). Given these estimates, the control law now takes the form

$$\bar{\boldsymbol{\tau}} = -\bar{\boldsymbol{K}}_P\boldsymbol{\varepsilon} - \bar{\boldsymbol{K}}_D\dot{\boldsymbol{\varepsilon}} - \boldsymbol{J}_{\mathcal{P}}^{-T}(\boldsymbol{Y}\hat{\boldsymbol{\theta}}_{\mathcal{P}} + \boldsymbol{\Psi}\hat{\boldsymbol{\delta}}_{\mathcal{P}}) \tag{37}$$

Using the preceding, the closed-loop tracking-error dynamics become

$$\boldsymbol{H}_{\mathcal{P}}^{*}\ddot{\boldsymbol{\varepsilon}} + (\bar{\boldsymbol{K}}_D + \boldsymbol{C}_P^{*})\dot{\boldsymbol{\varepsilon}} + \bar{\boldsymbol{K}}_P\boldsymbol{\varepsilon} = \boldsymbol{J}_{\mathcal{P}}^{-T}(\boldsymbol{Y}\tilde{\boldsymbol{\theta}}_{\mathcal{P}} + \boldsymbol{\Psi}\tilde{\boldsymbol{\delta}}_{\mathcal{P}}) \tag{38}$$

where the inertia parameter errors and the disturbance amplitude errors are defined as $\tilde{\boldsymbol{\theta}}_{\mathcal{P}} = \boldsymbol{\theta}_{\mathcal{P}}^{*} - \hat{\boldsymbol{\theta}}_{\mathcal{P}}$ and $\tilde{\boldsymbol{\delta}}_{\mathcal{P}} = \boldsymbol{\delta}_{\mathcal{P}}^{*} - \hat{\boldsymbol{\delta}}_{\mathcal{P}}$, respectively. The next step is to derive adaptive laws for $\hat{\boldsymbol{\theta}}_{\mathcal{P}}$ and $\hat{\boldsymbol{\delta}}_{\mathcal{P}}$ such that the proposed controller guarantees asymptotic stability despite the uncertainty in the inertia parameters and the external disturbance model. To develop the adaptive laws, a Lyapunov stability approach is used. We propose the following candidate Lyapunov function:

$$V = \tfrac{1}{2}\dot{\boldsymbol{\varepsilon}}^{T}\boldsymbol{H}_{\mathcal{P}}^{*}\dot{\boldsymbol{\varepsilon}} + \tfrac{1}{2}\boldsymbol{\varepsilon}^{T}\bar{\boldsymbol{K}}_P\boldsymbol{\varepsilon} + \tfrac{1}{2}\tilde{\boldsymbol{\theta}}_{\mathcal{P}}^{T}\Gamma_{T}^{-1}\tilde{\boldsymbol{\theta}}_{\mathcal{P}} + \tfrac{1}{2}\tilde{\boldsymbol{\delta}}_{\mathcal{P}}^{T}\Gamma_{\delta}^{-1}\tilde{\boldsymbol{\delta}}_{\mathcal{P}} \tag{39}$$

where $\Gamma_\theta = \Gamma_\theta^T \in R^{6\times 6}$ and $\Gamma_\delta = \Gamma_\delta^T \in R^{9\times 9}$ are symmetric, positive-definite, adaptation gain matrices. The time derivative of this Lyapunov function candidate is evaluated along the trajectories of Eq. (38) and is given by

$$\begin{aligned}\dot{V} = {} & \tfrac{1}{2}\dot{\boldsymbol{\varepsilon}}^{T}\left(\boldsymbol{H}_{\mathcal{P}}^{*} - 2\boldsymbol{C}_P^{*}\right)\dot{\boldsymbol{\varepsilon}} - \dot{\boldsymbol{\varepsilon}}^{T}\bar{\boldsymbol{K}}_D\dot{\boldsymbol{\varepsilon}} - \dot{\boldsymbol{\varepsilon}}^{T}\bar{\boldsymbol{K}}_P\boldsymbol{\varepsilon} \\ & + \dot{\boldsymbol{\varepsilon}}^{T}\boldsymbol{J}_{\mathcal{P}}^{-T}(\boldsymbol{Y}\tilde{\boldsymbol{\theta}}_{\mathcal{P}} + \boldsymbol{\Psi}\tilde{\boldsymbol{\delta}}_{\mathcal{P}}) + \dot{\boldsymbol{\varepsilon}}^{T}\bar{\boldsymbol{K}}_P\boldsymbol{\varepsilon} + \dot{\tilde{\boldsymbol{\theta}}}_{\mathcal{P}}^{T}\Gamma_{\delta}^{-1}\tilde{\boldsymbol{\theta}}_{\mathcal{P}} + \dot{\tilde{\boldsymbol{\delta}}}_{\mathcal{P}}^{T}\Gamma_{\delta}^{-1}\tilde{\boldsymbol{\delta}}_{\mathcal{P}}\end{aligned} \tag{40}$$

Noting that $\dot{\boldsymbol{H}}_{\mathcal{P}}^{*} - 2\boldsymbol{C}_P^{*}$ is skew-symmetric and following other simplifications, we obtain

$$\begin{aligned}\dot{V} = {} & -\dot{\boldsymbol{\varepsilon}}^{T}\bar{\boldsymbol{K}}_D\dot{\boldsymbol{\varepsilon}} + \left(\dot{\boldsymbol{\varepsilon}}^{T}\boldsymbol{J}_{\mathcal{P}}^{-T}\boldsymbol{Y} + \dot{\tilde{\boldsymbol{\theta}}}_{\mathcal{P}}^{T}\Gamma_{\theta}^{-1}\right)\tilde{\boldsymbol{\theta}}_{\mathcal{P}} \\ & + \left(\dot{\boldsymbol{\varepsilon}}^{T}\boldsymbol{J}_{\mathcal{P}}^{-T}\boldsymbol{\Psi} + \dot{\tilde{\boldsymbol{\delta}}}_{\mathcal{P}}^{T}\Gamma_{\delta}^{-1}\right)\tilde{\boldsymbol{\delta}}_{\mathcal{P}}\end{aligned} \tag{41}$$

The adaptive laws are then synthesized as follows:

$$\dot{\tilde{\boldsymbol{\theta}}}_{\mathcal{P}} = -\Gamma_\theta\boldsymbol{Y}^{T}\boldsymbol{J}_{\mathcal{P}}^{-1}\dot{\boldsymbol{\varepsilon}} \quad \text{or} \quad \dot{\hat{\boldsymbol{\theta}}}_{\mathcal{P}} = \Gamma_\theta\boldsymbol{Y}^{T}\boldsymbol{J}_{\mathcal{P}}^{-1}\dot{\boldsymbol{\varepsilon}} \tag{42}$$

and

$$\dot{\tilde{\boldsymbol{\delta}}}_{\mathcal{P}} = -\Gamma_\delta\boldsymbol{\Psi}^{T}\boldsymbol{J}_{\mathcal{P}}^{-1}\dot{\boldsymbol{\varepsilon}} \quad \text{or} \quad \dot{\hat{\boldsymbol{\delta}}}_{\mathcal{P}} = \Gamma_\delta\boldsymbol{\Psi}^{T}\boldsymbol{J}_{\mathcal{P}}^{-1}\dot{\boldsymbol{\varepsilon}} \tag{43}$$

Using the Eqs. (42) and (43) in Eq. (41), we obtain

$$\dot{V} = -\dot{\boldsymbol{\varepsilon}}^{T}\bar{\boldsymbol{K}}_D\dot{\boldsymbol{\varepsilon}} \le 0 \tag{44}$$

Because $\dot{V} \le 0$ and $V > 0$, we conclude that $\boldsymbol{\varepsilon}$, $\dot{\boldsymbol{\varepsilon}}$, $\tilde{\boldsymbol{\theta}}_{\mathcal{P}}$, and $\tilde{\boldsymbol{\delta}}_{\mathcal{P}} \in L_\infty$ (boundedness of signals); in addition, from Eq. (44), it follows that $\dot{\boldsymbol{\varepsilon}} \in L_2 \cap L_\infty$. Next, using Barbalat's lemma [17], it will be shown that $\dot{\boldsymbol{\varepsilon}} \to 0$ as $t \to \infty$.

Theorem 2. For the pursuer attitude dynamics described in Eq. (32), the choice of the control law in Eq. (37), together with the adaptation laws in Eqs. (42) and (43), guarantees asymptotic stability of the attitude tracking errors: that is, $(\boldsymbol{\varepsilon}, \dot{\varepsilon}) \to 0$ as $t \to \infty$.

Proof. Denoting $f(t) = \dot{V}$ as per Barbalat's lemma [17], we already know that $\dot{V}$ has a finite limit. Next, calculating $\ddot{V}$ yields

$$\begin{aligned}\ddot{V} = {} & -2\dot{\boldsymbol{\varepsilon}}^{T}\bar{\boldsymbol{K}}_D\ddot{\boldsymbol{\varepsilon}} = -2\dot{\boldsymbol{\varepsilon}}^{T}\bar{\boldsymbol{K}}_D\boldsymbol{H}_{\mathcal{P}}^{*-1}[-(\bar{\boldsymbol{K}}_D + \boldsymbol{C}_P^{*})\dot{\boldsymbol{\varepsilon}} \\ & - \bar{\boldsymbol{K}}_P\boldsymbol{\varepsilon} + \boldsymbol{J}_{\mathcal{P}}^{-T}(\boldsymbol{Y}\tilde{\boldsymbol{\theta}}_{\mathcal{P}} + \boldsymbol{\Psi}\tilde{\boldsymbol{\delta}}_{\mathcal{P}})]\end{aligned} \tag{45}$$

Because $\boldsymbol{\varepsilon}$, $\dot{\boldsymbol{\varepsilon}}$, $\boldsymbol{H}_{\mathcal{P}}^{*}$, $\boldsymbol{C}_P^{*}$, $\tilde{\boldsymbol{\theta}}_{\mathcal{P}}$, $\tilde{\boldsymbol{\delta}}_{\mathcal{P}}$, $\boldsymbol{Y}$, and $\boldsymbol{\Psi} \in L_\infty$, then $\ddot{V} \in L_\infty$. Because $\dot{V}$ is uniformly continuous, we conclude that $\dot{\boldsymbol{\varepsilon}} \to 0$ as $t \to \infty$.

To show that $\boldsymbol{\varepsilon} \to 0$ as $t \to \infty$, we follow the approach outlined in [24]. The closed-loop tracking-error dynamics in Eq. (38) represent a nonautonomous system. As a result, we use a theorem of Matrosov to show the stability. The theorem and its details are specified in the Appendix of [24] as well as in [25]. The application of this theorem boils down to showing that $\mathrm{d}^3V/\mathrm{d}t^3$ is negative-definite when restricted to M, the set of values of $(\boldsymbol{\varepsilon}, \dot{\boldsymbol{\varepsilon}})$ are such that $\dot{V} = 0$. Differentiating Eq. (44) twice, substituting the system dynamics, and evaluating it at M yields

$$\begin{aligned}\frac{\mathrm{d}^3V}{\mathrm{d}t^3} = {} & -2\left[\boldsymbol{H}_{\mathcal{P}}^{*-1}\left\{-\boldsymbol{K}_P\boldsymbol{\varepsilon} + \boldsymbol{J}_{\mathcal{P}}^{-T}(\boldsymbol{Y}\tilde{\boldsymbol{\theta}}_{\mathcal{P}} + \boldsymbol{\Psi}\tilde{\boldsymbol{\delta}}_{\mathcal{P}})\right\}\right]^{T}\bar{\boldsymbol{K}}_D \\ & \times \left[\boldsymbol{H}_{\mathcal{P}}^{*-1}\left\{-\boldsymbol{K}_P\boldsymbol{\varepsilon} + \boldsymbol{J}_{\mathcal{P}}^{-T}(\boldsymbol{Y}\tilde{\boldsymbol{\theta}}_{\mathcal{P}} + \boldsymbol{\Psi}\tilde{\boldsymbol{\delta}}_{\mathcal{P}})\right\}\right] < 0\end{aligned} \tag{46}$$

Based on the theorem of Matrosov, we finally conclude global asymptotic stability: that is, $\boldsymbol{\varepsilon} \to 0$ as $t \to \infty$ [24]. Thus, we have shown that $\boldsymbol{\varepsilon}$ and $\dot{\boldsymbol{\varepsilon}} \to 0$ as $t \to \infty$. □

Because the proof of global asymptotic stability requires us to satisfy certain key conditions, we present the theorem of Matrosov and the associated arguments in the Appendix.

V. Simulation Results

The numerical simulations performed to show the effectiveness of the proposed control approach were implemented using MATLAB and Simulink. The differential equations associated with the mathematical models of the pursuer, target, adaptive laws, and control laws discussed in previous sections were integrated using a fixed-time-step Runge–Kutta integration scheme (80 Hz). Several simulations were performed and only a representative set are presented in this section. The initial conditions and characteristics that remained the same in all of the simulations presented are as follows. The initial relative position and initial relative velocity of the pursuer with respect to the target are

$$\boldsymbol{r}^{\mathcal{O}}(0) = \begin{bmatrix} \frac{50}{\sqrt{2}} & 0 & \frac{50}{\sqrt{2}} \end{bmatrix}^{T} \text{ m}$$

and

$$\dot{\boldsymbol{r}}^{\mathcal{O}}(0) = [\,-0.5 \quad -0.5 \quad 0.5\,]^{T} \text{ m/s}$$

respectively. The desired relative distance was specified to be 5 m. The initial orientation of the LVLH frame with respect to the inertial frame is parameterized by

$$[\,\Omega \quad i \quad \omega\,] = [\,0 \quad 45\,\text{deg} \quad 0\,]$$

where Ω is the longitude of the ascending node, i is the inclination, and $\omega = \theta$ is the same as the latitude angle. The moment of inertia of the target and the pursuer spacecraft are assumed to be

$$\boldsymbol{H}_{\mathcal{T}} = \text{diag}[\,100 \quad 80 \quad 60\,] \text{ kgm}^2$$

In all of the simulations, the translational control and the rotational control accelerations were saturated at 20 m/s^2 and 100 deg/s^2, respectively. These are large values and may be impractical. However, the external disturbance force and torque magnitudes, initial condition errors, and target accelerations are quite large. The focus of the work was to illustrate the efficacy of the control and adaptive laws derived, and we did not try to optimize the control gains or the adaptation gains; they were arrived at by trial and error. Further, the control laws were implemented in a sample-and-hold fashion. The rotational and translational control laws were implemented at 16 and 8 Hz, respectively. Additionally, Gaussian white noise was injected into all the states used for feedback in the control laws. The noise corresponding to the attitude variables had a standard deviation of 0.1 units and that corresponding to the angular

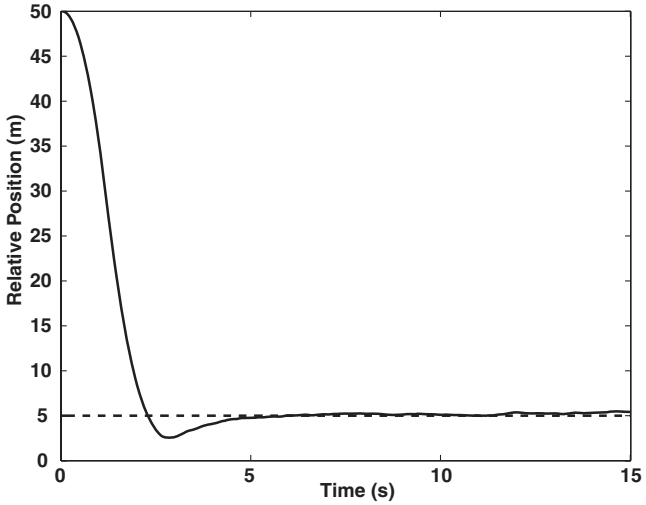

Fig. 4 Relative displacement time history.

velocity variables had 0.02 units. The standard deviation for the relative position was at 1 unit and that corresponding to the relative velocity was 0.1 unit. The parameters used for simulation are summarized in Table 1.

Figure 4 shows the relative displacement of the pursuer from the target. As can be seen, the control laws are very effective at bringing down the relative error smoothly. Figure 5 shows the alignment of the pursuer's axes with the desired frame, and Fig. 6 shows the angular errors between the pursuer and target reference frames. As desired, the angle between in $\hat{\boldsymbol{d}}_{\mathcal{T}}$ and $\hat{\boldsymbol{d}}_{\mathcal{P}}$ is 180 deg, thus meeting the control objective. This is simultaneously achieved with the relative position maintained at 5 m, as desired. The translational and rotational control histories are shown in Figs. 7 and 8, in which the sample-and-hold nature of the control law implementation is clearly seen. Finally, Fig. 9 shows that the pursuer tracks the virtual desired frame angular velocity, whereas the parameter errors remain bounded in the presence of persistent bounded disturbances (see Fig. 10). To ensure that the parameter errors remain bounded, the adaptive laws are modified in a fashion similar to that outlined in [17,26].

VI. Conclusions

The problem of motion synchronization of free-flying robotic spacecraft and serviceable floating objects in space was studied. A

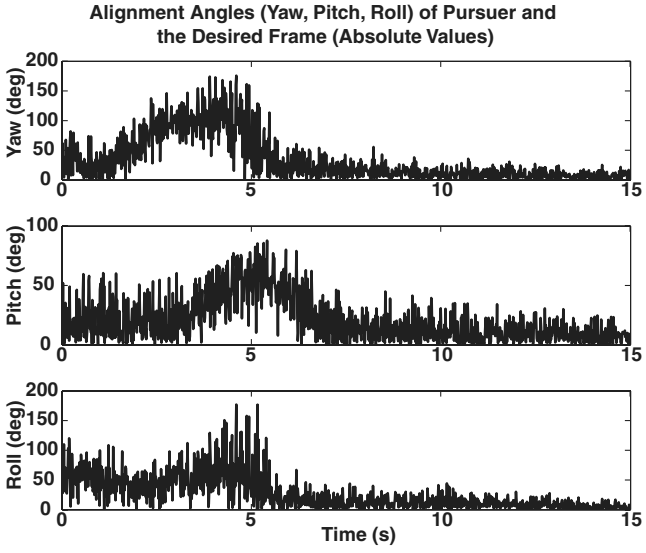

Fig. 5 Pursuer's alignment angles with the virtual desired frame.

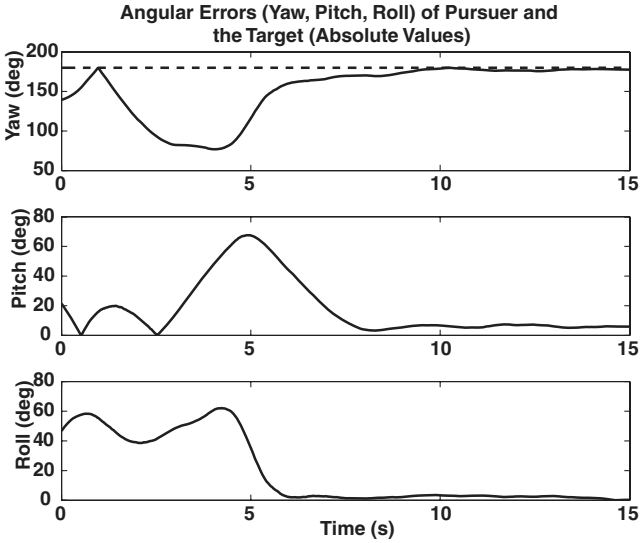

Fig. 6 Pursuer's orientation with respect to the target.

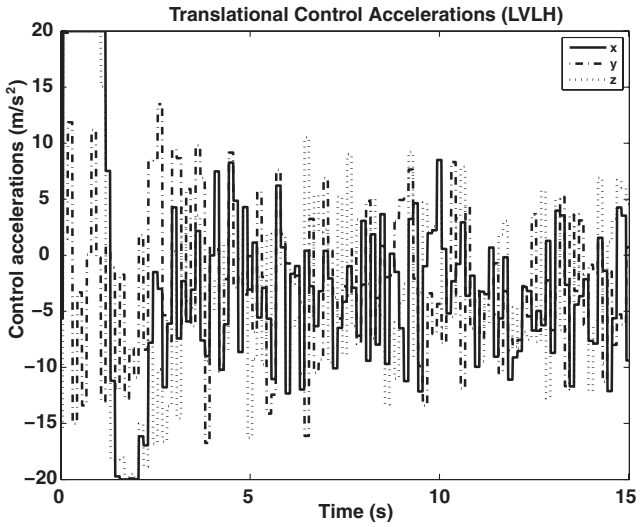

Fig. 7 Translational control history.

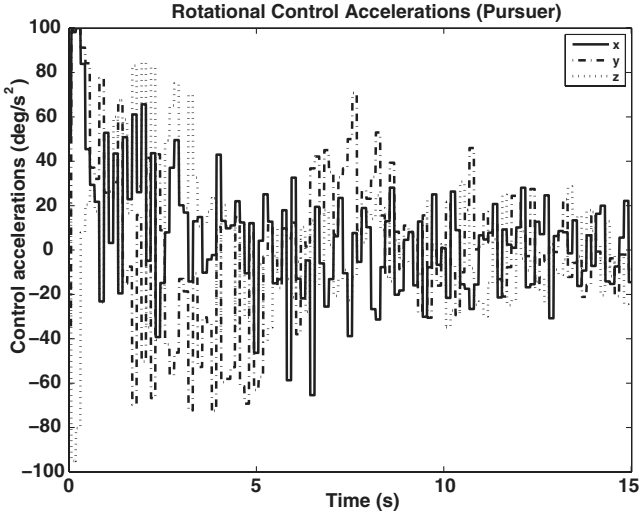

Fig. 8 Rotational control history.

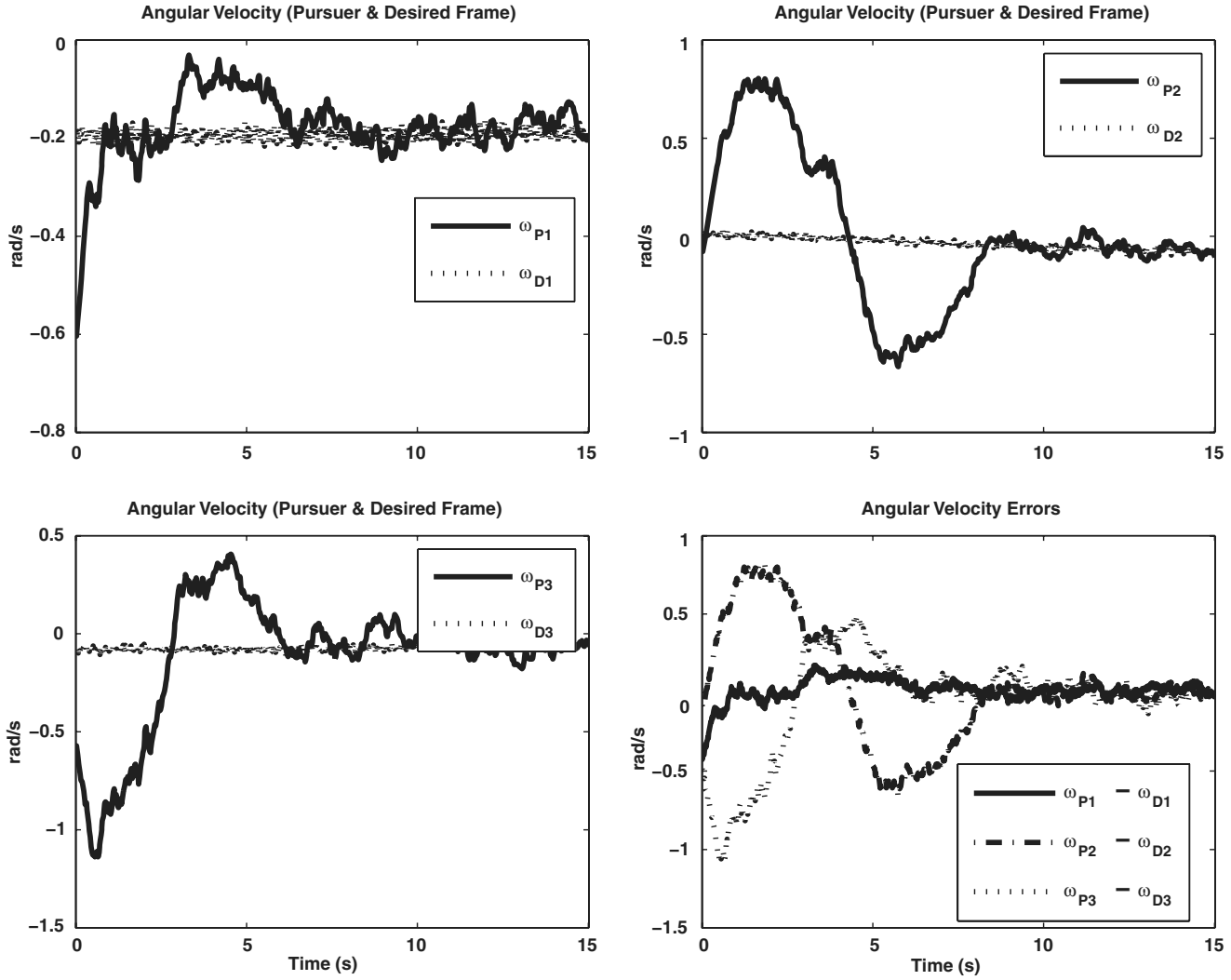

Fig. 9 Desired frame angular velocity tracking-error history.

coupled synchronization strategy was developed, wherein one maneuver aimed at maintaining a constant relative separation, with the relative position vector directed along the docking port of the target. An adaptive attitude control law was developed that reorients the pursuer to direct its docking port along the relative position vector. The control laws show acceptable tracking accuracies for synchronization, as well as in the presence of unmodeled disturbances and uncertain inertia parameters of the pursuer. Additionally, an adaptive disturbance compensation mechanism was devised to mitigate the effects due to the aforementioned disturbances. Finally, the stability of the control law was demonstrated via a Lyapunov analysis and Matrosov's theorem. The performance of the closed loop was verified through representative numerical simulations.

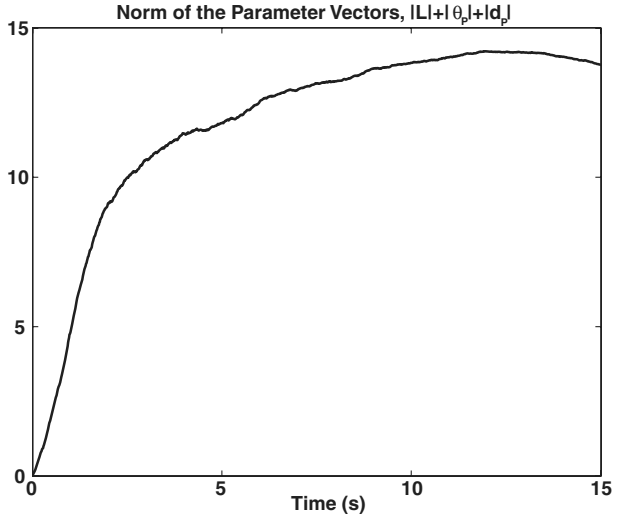

Fig. 10 Sum of the norms of the parameters.

Appendix: Application of Matrosov's Theorem

This Appendix summarizes the developments in [24] and verifies the conditions for the application of the theorem of Matrosov.

Definition: A continuous function α: $R_+ \to R_+$ is said to be of class $\mathcal{K}$ if 1) $\alpha(p)$ is strictly increasing and 2) $\alpha(0) = 0$.

We state Matrosov's theorem without the proof.

Theorem 3 (Matrosov). Let $\Omega \in R^n$ be an open connected region in R^n containing the origin. If there exist two C^1 functions V: $[t_0, \infty) \times \Omega \to R$ and W: $[t_0, \infty) \times \Omega \to R$; a C^0 function V^*: $\Omega \to R$; and three functions a, b, and c of class $\mathcal{K}$, such that for every $(x, t) \in [t_0, \infty) \times \Omega$,

1) $a(\|x\|) \le V(t, x) \le b(\|x\|)$.

2) $\dot{V}(t, x) \le V^*x \le 0$. Define $M \triangleq \{x \in \Omega | V^*x - 0\}$.

3) $|W(t, x)|$ is bounded.

4) $\max(d(x, M), |\dot{W}(t, x)|) \ge c(\|x\|)$.

5) $\|f(t, x)\|$ is bounded.

Choosing $\alpha > 0$ such that $\bar{B}_\alpha \subset \Omega$, define for all $t \in [t_0, \infty)$

$$V_{t,\alpha}^{-1} = \{x \in \Omega \colon V(t, x) \le a(\alpha)\}$$

Table 1 Simulation parameters

Description	Value[a]	Units
Orbit of target	Elliptical, eccentricity is 0.1375	N/A
$\boldsymbol{\omega}^{\mathcal{T}}_{\mathcal{TN}}(0)$	$[10 \quad 10 \quad 10]^T + \boldsymbol{\eta}_1, \boldsymbol{\eta}_1 \sim \mathcal{N}(0, 2)$	deg/s
$\boldsymbol{\omega}^{\mathcal{P}}_{\mathcal{PN}}(0)$	$\boldsymbol{\omega}^{\mathcal{P}}_{\mathcal{DN}}(0) + \boldsymbol{\eta}_2, \boldsymbol{\eta}_2 \sim \mathcal{N}(0, \|\boldsymbol{\omega}^{\mathcal{P}}_{\mathcal{DN}}(0)\|)$	deg/s
$\boldsymbol{\sigma}_{\mathcal{T}}(0)$	E313ToMRP($[\Omega \quad i \quad \omega]$)	MRP
$\boldsymbol{\sigma}_{\mathcal{P}}(0)$	$\boldsymbol{\sigma}_{\mathcal{D}}(0) + \boldsymbol{\eta}_3, \boldsymbol{\eta}_3 \sim \mathcal{N}(0, \|\boldsymbol{\sigma}_{\mathcal{D}}(0)\|)$	MRP
Translational disturbances	$(1 + \cos(\lambda t) + \sin(\lambda t))\boldsymbol{\eta}_4, \boldsymbol{\eta}_4 \sim \mathcal{N}(0, 1)$	m/s^2
Adaptive gain (translation)	$\Gamma = 5I_{3\times3}$	N/A
ν modification	$\nu = 0.1$	N/A
Adaptive gain (rotation)	$\Gamma_\Psi = 0.15I_{9\times9}$	N/A
Adaptive gain (rotation)	$\Gamma_Y = 1000I_{6\times6}$	N/A
Translational law gains	$\boldsymbol{K}_I = 0.001I_{3\times3}, \boldsymbol{K}_P = 10I_{3\times3}, \boldsymbol{K}_D = 10I_{3\times3}$	N/A
Rotational law gains	$\bar{\boldsymbol{K}}_I = I_{3\times3}, \bar{\boldsymbol{K}}_P = 800I_{3\times3}, \bar{\boldsymbol{K}}_D = 600I_{3\times3}$	N/A

[a]Note that λ is the instantaneous latitude rate, E313ToMRP implies conversion of the 3–1–3 Euler angle sequence to MRP, $\boldsymbol{\sigma}_{\mathcal{D}}$ is the desired MRP derived from the target orientation, and $\boldsymbol{\omega}^{\mathcal{P}}_{\mathcal{DN}}$ is the desired angular velocity derived from the target.

Then for all $x_0 \in V^{-1}_{t,\alpha}$ $[x(t) \to 0]$ uniformly in t_0 and x_0 as $t \to \infty$, the origin is uniformly asymptotically stable.

Proof. See Rouche et al. [27]. □

Remarks. Condition 1 is a common requirement in Lyapunov analysis for guaranteeing uniform stability. The region defined by M in condition 2 is important. Conditions 3 and 4 ensure that near M and far away from the origin, the rate of change of a *second bounded auxiliary function* is of constant sign and bounded away from zero. This further ensures that the state converges to the origin. To verify condition 4, another lemma is provided in [24].

We now show that the aforementioned conditions are satisfied for the closed-loop attitude error dynamics in the present case. Checking conditions 1 and 2 is fairly straightforward for the Lyapunov function candidate chosen in Eq. (39). We have already shown the boundedness of the tracking errors, error rates, and parameter errors. Also, with $\boldsymbol{H}^*_{\mathcal{P}}$ being twice differentiable because $\boldsymbol{\sigma}_{\mathcal{P}}$ is bounded, the covariant tensors [24] associated with the partial differentiation of $\boldsymbol{H}^*_{\mathcal{P}}$ with respect to $\boldsymbol{\sigma}_{\mathcal{P}}$ are bounded. Further, $\ddot{\boldsymbol{\varepsilon}}$ is continuous in the tracking error and depends continuously on time through $\boldsymbol{\varepsilon}$ and $\dot{\boldsymbol{\varepsilon}}$, which are bounded. For checking condition 3, we define

$$W(\boldsymbol{\varepsilon}, \dot{\boldsymbol{\varepsilon}}, t) \triangleq \ddot{V} = -2\dot{\boldsymbol{\varepsilon}}\bar{\boldsymbol{K}}_D\ddot{\boldsymbol{\varepsilon}}$$

Clearly, W is bounded. To check condition 4, we follow the lemma in [24] (p. 1709). We compute $\dot{W} = (\mathrm{d}^3V/\mathrm{d}t^3)$:

$$\begin{aligned}\frac{\mathrm{d}^3V}{\mathrm{d}t^3} &= -\ddot{\boldsymbol{\varepsilon}}^T\bar{\boldsymbol{K}}_D\boldsymbol{H}^{*-1}_{\mathcal{P}}\{-(\bar{\boldsymbol{K}}_D + \boldsymbol{C}^*_P)\dot{\boldsymbol{\varepsilon}} \\ &\quad - \bar{\boldsymbol{K}}_P\boldsymbol{\varepsilon} + \boldsymbol{J}^{-T}_{\mathcal{P}}(\boldsymbol{Y}\tilde{\boldsymbol{\theta}}_{\mathcal{P}} + \boldsymbol{\Psi}\tilde{\boldsymbol{\delta}}_{\mathcal{P}})\} - \dot{\boldsymbol{\varepsilon}}^T\bar{\boldsymbol{K}}_D\frac{\mathrm{d}}{\mathrm{d}t} \\ &\quad \times [\boldsymbol{H}^{*-1}_{\mathcal{P}}\{-(\bar{\boldsymbol{K}}_D + \boldsymbol{C}^*_P)\dot{\boldsymbol{\varepsilon}} - \bar{\boldsymbol{K}}_P\boldsymbol{\varepsilon} + \boldsymbol{J}^{-T}_{\mathcal{P}}(\boldsymbol{Y}\tilde{\boldsymbol{\theta}}_{\mathcal{P}} + \boldsymbol{\Psi}\tilde{\boldsymbol{\delta}}_{\mathcal{P}})\}] \quad \text{(A1)}\end{aligned}$$

Notice that all terms on the RHS of the preceding equation are continuous with respect to $\boldsymbol{\varepsilon}$ and $\dot{\boldsymbol{\varepsilon}}$ and depend continuously on time through a bounded function. Thus, it can be shown that $(\mathrm{d}/\mathrm{d}t)\ddot{\boldsymbol{\varepsilon}}$ is continuous in the tracking error and depends on time continuously through a bounded function. Because the maximum singular value of the inertia matrix $\boldsymbol{H}^*_{\mathcal{P}}$ is assumed bounded, condition 4 of the theorem is verified. Because $\boldsymbol{\sigma}_{\mathcal{P}}$ and $\dot{\boldsymbol{\sigma}}_{\mathcal{P}}$ are bounded and $\boldsymbol{H}^*_{\mathcal{P}}\ddot{\boldsymbol{\sigma}}_{\mathcal{P}}$ is continuous with respect to these variables and the tracking errors, the system dynamics are bounded. Thus, through these relatively straightforward arguments, we show that all conditions Matrosov's theorem are satisfied. Also, for arbitrary initial conditions, one can choose condition 1 to find an α and Ω such that the initial conditions are contained in $V^{-1}_{t_0,\alpha}$. Hence, by application of Matrosov's theorem, the origin is globally asymptotically stable.

References

[1] Matsumoto, S., Ohkami, Y., Wakabayashi, Y., Oda, M., and Ueno, H., "Satellite Capturing Strategy Using Agile Orbital Servicing Vehicle, Hyper-OSV," *Proceedings of the IEEE International Conference on Robotics and Automation*, Inst. of Electrical and Electronics Engineers, Piscataway, NJ, 2002, pp. 2309–2314.

[2] Lichter, M. D., and Dubowsky, S., "State, Shape, and Parameter Estimation of Space Objects from Range Images," *Proceedings of the 2004 IEEE International Conference on Robotics and Automation (ICRA 2004)*, Inst. of Electrical and Electronics Engineers, Piscataway, NJ, Apr. 2004, pp. 2974–2979.

[3] Jacobsen, S., Zhu, C., Lee, C., and Dubowsky, S., "Planning of Safe Kinematic Trajectories for Free-Flying Robots Approaching an Uncontrolled Spinning Satellite," *2002 ASME Design Engineering Technical Conferences & Computers and Information in Engineering Conference*, American Society of Mechanical Engineers, New York, 2002, pp. 1–7.

[4] Tsuda, Y., and Shinichi, N., "New Attitude Motion Following Control Algorithm for Capturing Tumbling Object in Space," *Acta Astronautica*, Vol. 53, No. 11, 2003, pp. 847–861. doi:10.1016/S0094-5765(02)00213-8

[5] Tsuda, Y., Fujiwara, T., Nakamura, T., and Nakasuka, S., "The Attitude Control for Motion Synchronization to Capture Free-Flying Object," *Proceedings of the 8th Workshop on Astrodynamics and Flight Mechanics*, Inst. of Space and Astronautical Science, Tokyo, 1998, pp. 348–354.

[6] Isao, K., Mokuno, M., Toru, K., and Suziki, T., "Result of Autonomous Rendezvous Docking Experiment of Engineering Test Satellite-VII," *Journal of Spacecraft and Rockets*, Vol. 38, No. 1, Jan.–Feb. 2001, pp. 105–111.

[7] Schaub, H., and Junkins, J. L., *Analytical Mechanics of Space Systems*, AIAA Education Series, AIAA, Reston, VA, 2003, Chaps. 3, 8.

[8] Singla, P., Subbarao, K., Hughes, D., and Junkins, J. L., "Structured Model Reference Adaptive Control for Vision Based Spacecraft Rendezvous and Docking Problem," AAS/AIAA Space Flight Mechanics Meeting, Ponce, Puerto Rico, American Astronautical Society Paper 03-103, Feb. 2003.

[9] Shuster, M. D., "A Survey of Attitude Representations," *Journal of the Astronautical Sciences*, Vol. 41, No. 4, Oct.–Dec. 1993, pp. 439–517.

[10] Singla, P., Subbarao, K., and Junkins, J. L., "Output Feedback Based Adaptive Control for Spacecraft Rendezvous and Docking Under Measurement Uncertainties," *Journal of Guidance, Control, and Dynamics*, Vol. 29, No. 4, 2006, pp. 892–902.

[11] Schaub, H., Akella, M. R., and Junkins, J. L., "Adaptive Control of Nonlinear Attitude Motions Realizing Linear Closed Loop Dynamics,"*Journal of Guidance, Control, and Dynamics*, Vol. 24, No. 1, Jan.–Feb. 2001, pp. 95–100,.

[12] Schaub, H., Akella, M. R., and Junkins, J. L., "Adaptive Realization of Linear Closed Loop Tracking Dynamics in the Presence of Large System Model Errors," *Journal of the Astronautical Sciences*, Vol. 48, No. 4, Oct.–Dec. 2000, pp. 537–551.

[13] Paielli, R. A., and Bach, R. E., "Attitude Control with Realization of Linear Error Dynamics," *Journal of Guidance, Control, and Dynamics*, Vol. 16, No. 1, 1993, pp. 182–189.

[14] Gennaro, S. D., "Adaptive Robust Stabilization of Spacecraft in Presence of Disturbances," *Journal of Optimization Theory and Applications*, Vol. 98, No. 3, 1998, pp. 545–568. doi:10.1023/A:1022667811792

[15] Tanygin, S., "Generalization of Adaptive Attitude Tracking,"AIAA/AAS Astrodynamics Specialist Conference and Exhibit, Monterey, CA, AIAA Paper 2002-4833, Aug. 2002.

[16] Gantmacher, F. R., *The Theory of Matrices*, Vol 1, Chelsea Publishing, NY, 1977, pp. 353–354.

[17] Ioannou, P. A., and Sun, J., *Stable and Robust Adaptive Control*, Prentice–Hall, Upper Saddle River, NJ, 1995.

[18] Subbarao, K., "The Attitude Control Problem, Re-Visited," AAS John L. Junkins Astrodynamics Symposium, College Station, TX, American Astronautical Society Paper 03-263, 2003.

[19] Stoer, J., and Bulirsch, R., *Introduction to Numerical Analysis*, Springer–Verlag, New York, 1993.

[20] Zhou, K., and Doyle, J. C., *Essentials of Robust Control*, Prentice–Hall, Upper Saddle River, NJ, 1998.

[21] Wong, H., de Queiroz, M. S., and Kapila, V., "Adaptive Tracking Control Using Synthesized Velocity from Attitude Measurements," *Journal of Guidance, Control, and Dynamics*, Vol. 24, No. 6, 2001.

[22] Subbarao, K., "Structured Adaptive Model Inversion (SAMI): Theory and Applications to Trajectory Tracking for Non-Linear Dynamical Systems," Ph.D. Thesis, Dept. of Aerospace Engineering, Texas A&M Univ., College Station, TX, Aug. 2001.

[23] Ahmed, J., Coppola, V. T., and Bernstein, D. S., "Adaptive Asymptotic Tracking of Spacecraft Attitude Motion with Inertia Matrix Identification," *Journal of Guidance, Control, and Dynamics*, Vol. 21, No. 5, Sept.–Oct. 1998, pp. 684–691.

[24] Paden, B., and Panja, R., "Globally Asymptotically Stable 'PD$^+$' Controller for Robot Manipulators," *International Journal of Control*, Vol. 47, No. 6, 1988, pp. 1697–1712. doi:10.1080/00207178808906130

[25] Loria, A., Panteley, E., Popovic, D., and Teel, A. R., "A Nested Matrosov Theorem and Persistency of Excitation for Uniform Convergence in Stable Nonautonomous Systems," *IEEE Transactions on Automatic Control*, Vol. 50, No. 2, 2005, pp. 183–198. doi:10.1109/TAC.2004.841939

[26] Subbarao, K., and Junkins, J. L., "Structured Model Reference Adaptive Control for a Class of Nonlinear Systems," *Journal of Guidance, Control, and Dynamics*, Vol. 26, No. 4, July–Aug. 2003, pp. 551–557.

[27] Rouche, N., Habets, P., and Laloy, M., *Stability Theory by Liapunov's Direct Method*, Springer–Verlag, New York, 1977.